Electronic Supplementary Information

S-doped Au/Pd/Pt aerogels becoming Superior HER catalysts by Constructing Atomic-scale Au-Pd-Pt Diffuse Interfaces

Yongchan Fan, Shuai Jiang, Qi Xu, Mengjiao Hao, Jiayi Hou, He Tian and Haibing Xia**

Experimental Section

Materials. Chloroauric acid tetrahydrate ($HAuCl_4 \cdot 4H_2O$, 99%), L-ascorbic acid (AA, 99%), trisodium citrate dihydrate ($Na_3C_6H_5O_7 \cdot 2H_2O$, 99%), sodium borohydride ($NaBH_4$, 99%) were purchased from Sinopharm Chemical Reagent Co., Ltd. (Shanghai, China). Reduced glutathione (GSH, 98%) was purchased from Aladdin (Shanghai, China). Lead(II) chrolide ($PbCl_2$) and Nafion solution (5 wt%) were purchased from Sigma-Aldrich Co. LLC. Sodium tetrachloropalladate(II) hydrate (Na_2PdCl_4, 99%), potassium hexachloroplatinate (K_2PtCl_6, 99%), commercial Pt/C catalysts (nominally 20% on carbon black) and commercial Pd/C catalysts (nominally 10% on carbon black) were purchased from Alfa Aesar (Tianjin, China). All the chemicals were used as received without other treatment. All the experiments used Milli-Q water with a resistivity of 18.2 MΩ cm. The aqua regia (3:1= v/v HCl (37%): HNO_3 (65%) solution) was used to clean all glassware thoroughly. And all glassware was washed completely with Milli-Q water before use. (***Caution***: *Aqua regia are dangerous and must be used with extreme care; never store these solutions in closed containers.*)

Instrumental Characterizations.

The JEOL JEM-2100F transmission electron microscope was used to characterize the morphology of the samples. The transmission electron microscope (TEM) images and high-resolution transmission electron microscope (HR-TEM) images of the samples was obtained at the acceleration voltage of 200 kV.

High-angle annular dark-field-scanning transmission electron microscopy (HAADF-STEM) and HAADF-STEM-EDS mapping images were obtained by a JEOL JEM-2100F transmission electron microscope with a STEM unit.

The X-ray diffraction (XRD) pattern of the samples was obtained on a PANalytical X'pert3 powder diffractometer (40 kV, 40 mA) using a Cu Kα radiation (λ= 0.15418 nm) and was recorded in the range from 20° to 90° (2θ) with a step length of 0.08°.

X-ray Photoelectron Spectroscopy (XPS) spectra of different samples were obtained by Thermo Fisher Scientific ESCALAB 250 XPS spectrometer with a monochromatic Al Kα X-ray radiation.

Electrochemical Characterizations.

CO stripping experiments. CO stripping experiments were performed on a standard three-electrode system using a CHI 660D workstation at room temperature. An Ag/AgCl

electrode and a Hg/HgO electrode was used as the reference electrode in acidic media and in alkaline media, respectively. A Pt wire was used as the counter electrode.

Before the CO stripping experiments under acidic media, the H_2SO_4 solution (0.5 M) has to be deoxygenated by bubbling with high-purity N_2 for at least 30 min, followed by continuous CO bubbling for another 30 min. Then, the CO stripping experiments were performed by holding the electrode potential at 0.24 V (*vs.* RHE) in high-purity CO-saturated H_2SO_4 solution with continuous CO bubbling for 1 000 s. Next, the H_2SO_4 solution was purged out thoroughly by bubbling with high-purity N_2 for 30 min to guarantee the complete elimination of CO. Eventually, two consecutive CV curves were recorded at the potential range from 0 V to 1.4 V (*vs.* RHE) at a scan rate of 50 mV s^{-1}. All potentials were transferred to the reversible hydrogen electrode (RHE) on the basis of $E_{RHE} = E_{Ag/AgCl} + 0.0591 \times pH + 0.198$.

Before the CO stripping experiments under alkaline media, the KOH solution (0.1 M) has to be deoxygenated by bubbling with high-purity N_2 for at least 30 min, followed by continuous CO bubbling for another 30 min. Then, the CO stripping experiments were performed by holding the electrode potential at 0.147 V (*vs.* RHE) in high-purity CO-saturated KOH solution with continuous CO bubbling for 1 000 s. Next, the KOH solution was purged out thoroughly by bubbling with high-purity N_2 for 30 min to guarantee the complete elimination of CO. Eventually, two consecutive CV curves were recorded at the potential range from 0 V to 1.4 V (*vs.* RHE) at a scan rate of 50 mV s^{-1}. All potentials were transferred to the reversible hydrogen electrode (RHE) on the basis of $E_{RHE} = E_{Hg/HgO} + 0.0591 \times pH + 0.098$.

HER measurements. Electrochemical investigations towards the HER were also performed on a standard three-electrode system using a CHI 660D workstation at room temperature. An Ag/AgCl electrode (saturated KCl) and a Hg/HgO electrode (saturated KCl) was used as the reference electrode in acidic media and in alkaline media, respectively. A graphite rod was used as the counter electrode. All potentials were converted to the RHE according to $E_{RHE} = E_{Ag/AgCl} + 0.0591 \times pH + 0.197$ (in acidic media) and $E_{RHE} = E_{Hg/HgO} + 0.0591 \times pH + 0.098$ (in alkaline media).

Glass carbon electrodes (GCEs) (3 mm in diameter, 0.07065 cm^2 in geometric area) were used as the working electrode for the HER. The GCEs were coated with the as-prepared $S_{6.5}$-doped $Au_{77.6}/Pd_{0.8}/Pt_{15.1}$ aerogel according to the same method used in the ORR test. However, the Pt loading of all samples on the GCEs for the HER was reduced to 6 μg_{Pt} cm^{-2}. For comparison, the GCEs modified with commercial Pt/C catalysts were prepared with a Pt loading of 21 μg_{Pt} cm^{-2}.

Prior to any HER measurement, the electrolyte solution (0.5 M H_2SO_4 or 0.1 M KOH) was first purged with high purity N_2 for 30 min. CV measurements were conducted in a N_2-saturated 0.5 M H_2SO_4 (0.1 M KOH) solution with a scan rate of 50 mV s^{-1}. LSV measurements were conducted in a N_2-saturated 0.5 M H_2SO_4 (0.1 M KOH) solution with a scan rate of 5 mV s^{-1}, and vigorous stirring is necessary to avoid the impact of H_2 bubbles on the catalyst surfaces.

ADTs were to evaluate the stability of the catalyst within the cycling potential ranging from 0.133 to 0.27 V (*vs.* RHE) with a scan rate of 100 mV s^{-1} for 5k cycles. Note that all the LSV curves were iR-corrected.

The electrochemical impedance spectroscopy (EIS) measurements were carried out in the frequency range from 100 kHz to 0.1 Hz with an amplitude of the sinusoidal wave was 5 mV.

Figure S1. TEM images of a series of S-doped AuPdPt aerogels prepared under different molar ratios of Pd(II)-to-Pt(IV): 5:6 (a), 6:7 (b), and 2:8 (c).

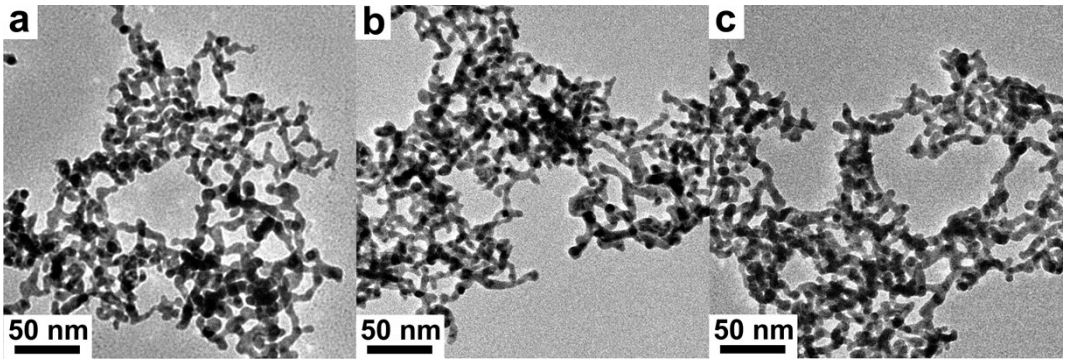

Figure S2. LSV curves (A), histograms of η_{10} values (B) and Tafel slopes (C) of a series of S-doped AuPdPt aerogels towards the alkaline HER (0.1 M KOH), which were prepared under different molar ratios of Pd(II)-to-Pt(IV): 5:4.5 (a), 5:5 (b), 5:5.5 (c), 5:6 (d), 5:6.5 (e), and 5:7 (f).

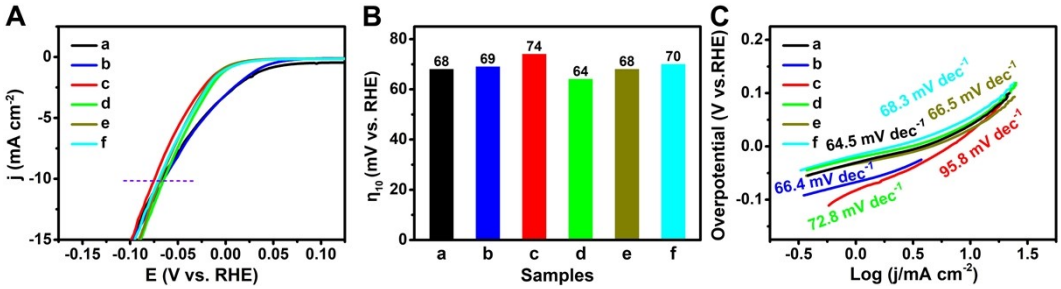

The S-doped AuPb aerogel as the template was firstly prepared. Then, these S-doped AuPdPt aerogels were synthesized by the same procedure except that the molar ratios of Pd(II)-to-Pt(IV) precursors were changed from 5:4.5 to 5:5, 5:5.5, 5:6, 5:6.5 and 5:7 accordingly. As shown in **Figure S2A and S2B**, the overpotential at -10 mA cm^{-2} (η_{10}) towards the HER in alkaline media of these S-doped AuPdPt aerogels are 68, 69, 74, 64, 68 and 70 mV (*vs.* RHE), respectively. Their Tafel slope are 64.5, 66.4, 95.8, 72.8, 66.5, and 68.3 mV dec^{-1} (**Figure S2C**).

Figure S3. LSV curves (A and D), histograms of η_{10} values (B and E) and Tafel slopes (C and F) of a series of S-doped AuPdPt aerogels towards the alkaline HER (0.1 M KOH) and the acidic HER (0.5 M H_2SO_4), respectively, which were prepared under different molar ratios of Pd(II)-to-Pt(IV): 6:4 (a), 6:5 (b), 6:6 (c), and 6:7 (d).

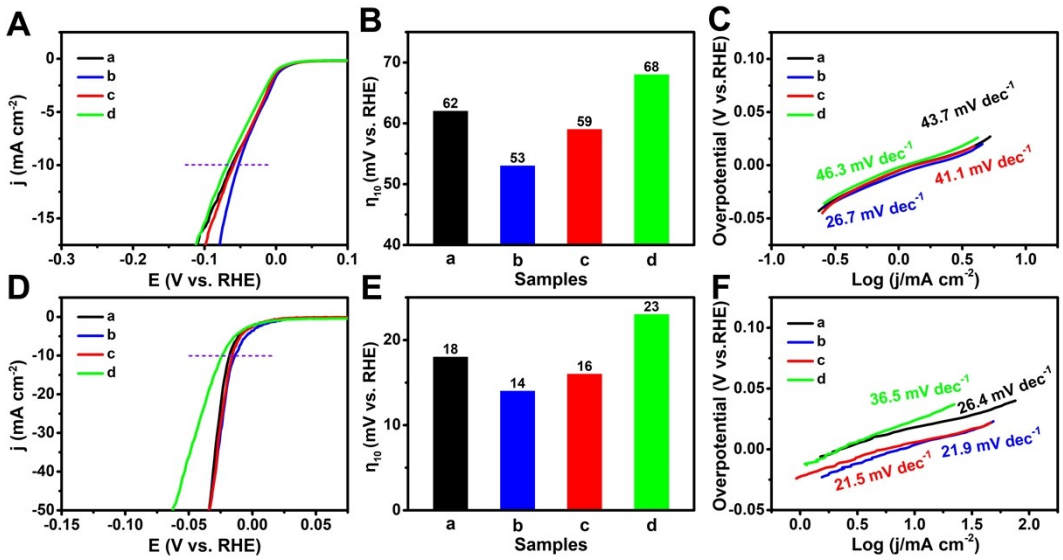

These S-doped AuPdPt aerogels were obtained by the same procedure except that the molar ratios of Pd(II)-to-Pt(IV) precursors were changed from 6:4 to 6:5, 6:6, and 6:7 accordingly. As shown in **Figure S3A and S3B**, their η_{10} values towards the HER in alkaline media are 62, 53, 59 and 68 mV (*vs.* RHE), respectively. And their Tafel slope are 43.7, 26.7, 41.1 and 46.3 mV dec^{-1} **(Figure S3C)**. Moreover, as shown in **Figure S3D and S3E**, their η_{10} values towards the HER in acidic media are 18, 14, 16 and 23 mV (*vs.* RHE), respectively. And Their Tafel slope are 26.4, 21.9, 21.5 and 36.5 mV dec^{-1} **(Figure S3F)**.

Figure S4. LSV curves (A and D), histograms of η_{10} values (B and E), Tafel slopes (C and F) of a series of S-doped AuPdPt aerogels towards the alkaline HER (0.1 M KOH) and the acidic HER (0.5 M H_2SO_4), respectively, which were prepared under different molar ratios of Pd(II)-to-Pt(IV): 7:4 (a), 7:5 (b), 7:6 (c), and 7:7 (d).

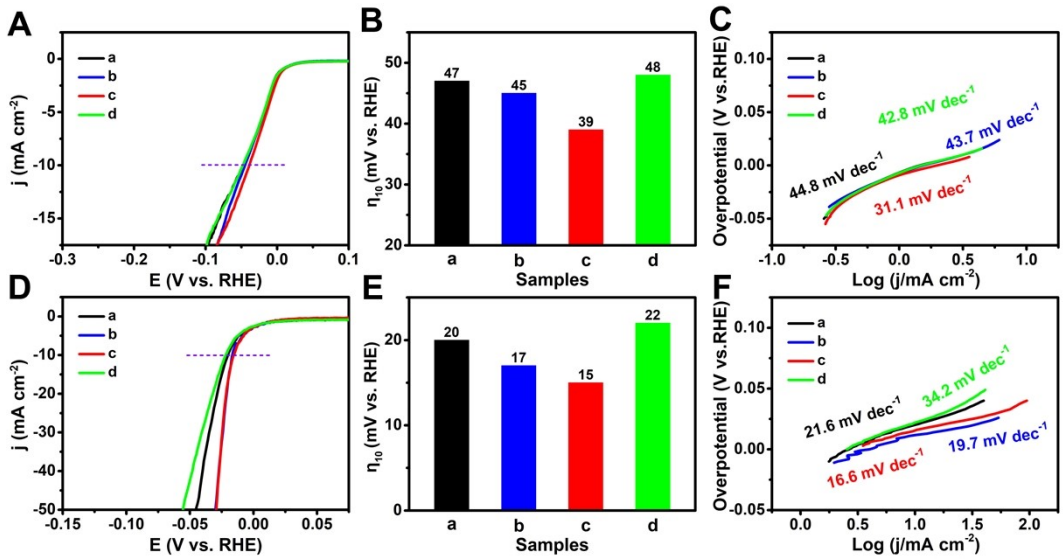

A series of S-doped AuPdPt aerogels were obtained by the same procedure except that the molar ratios of Pd(II)-to-Pt(IV) precursors were changed from 7:4 to 7:5, 7:6, and 7:7 accordingly. As shown in **Figure S4A and S4B**, their η_{10} values towards the HER in alkaline media are 47, 45, 39 and 48 mV (*vs.* RHE), respectively. And their Tafel slope are 44.8, 43.7, 31.1 and 42.8 mV dec^{-1} **(Figure S4C)**. Moreover, as shown in **Figure S4D and S4E**, their η_{10} values towards the HER in acidic medial are 20, 17, 15 and 22 mV (*vs.* RHE), respectively. And their Tafel slope are 21.6, 19.7, 16.6 and 34.2 mV dec^{-1} **(Figure S4F)**.

Figure S5. LSV curves (A and D), histograms of η_{10} values (B and E), Tafel slopes (C and F) of a series of S-doped AuPdPt aerogels towards the alkaline HER (0.1 M KOH) and the acidic HER (0.5 M H_2SO_4), respectively, which were prepared under different molar ratios of Pd(II)-to-Pt(IV): 4:6 (a), 3:7 (b), 2:8 (c), and 1:9 (d).

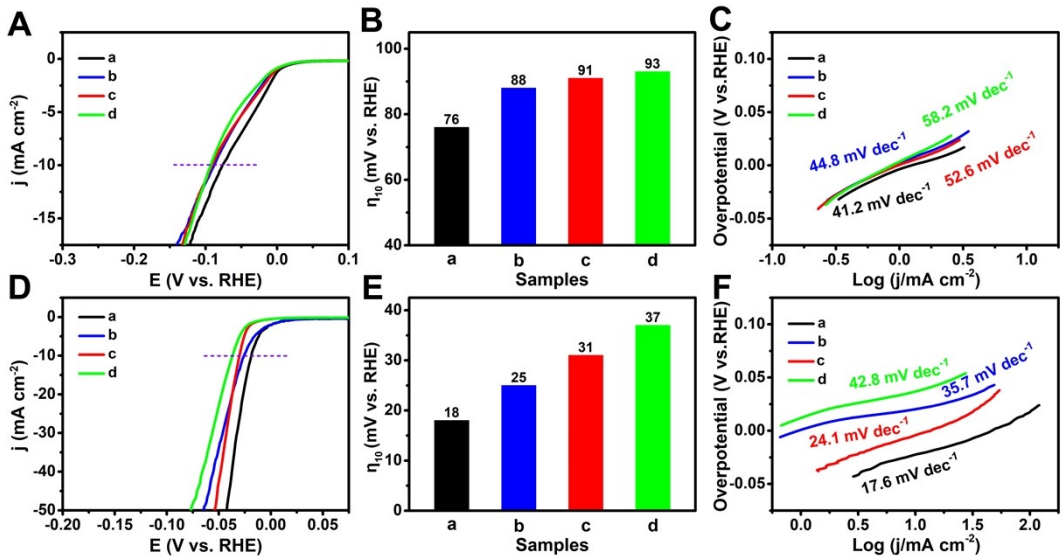

These S-doped AuPdPt aerogels were obtained by the same procedure except that the molar ratios of Pd(II)-to-Pt(IV) precursors were changed from 4:6 to 3:7, 2:8, and 1:9 accordingly. As shown in **Figure S5A and S5B**, their η_{10} values towards the HER in alkaline media are 76, 88, 91 and 93 mV (*vs.* RHE), respectively. And their Tafel slope are 41.2, 44.8, 52.6 and 58.2 mV dec^{-1} **(Figure S5C)**. Moreover, as shown in **Figure S5D and S5E**, their η_{10} values towards the HER in acidic media are 18 mV, 25 mV, 31 mV, and 37 mV (*vs.* RHE), respectively. And their Tafel slope are 17.6, 35.7, 24.1 and 42.8 mV dec^{-1} **(Figure S5F)**.

Figure S6. TEM images of a series of S-doped AuPdPt aerogels prepared under different molar ratios of Pd(II)-to-Pt(IV): 1:9 (a), 1:10 (b), 1:15 (c), 1:20 (d), 1:22 (e), and 1:24 (f).

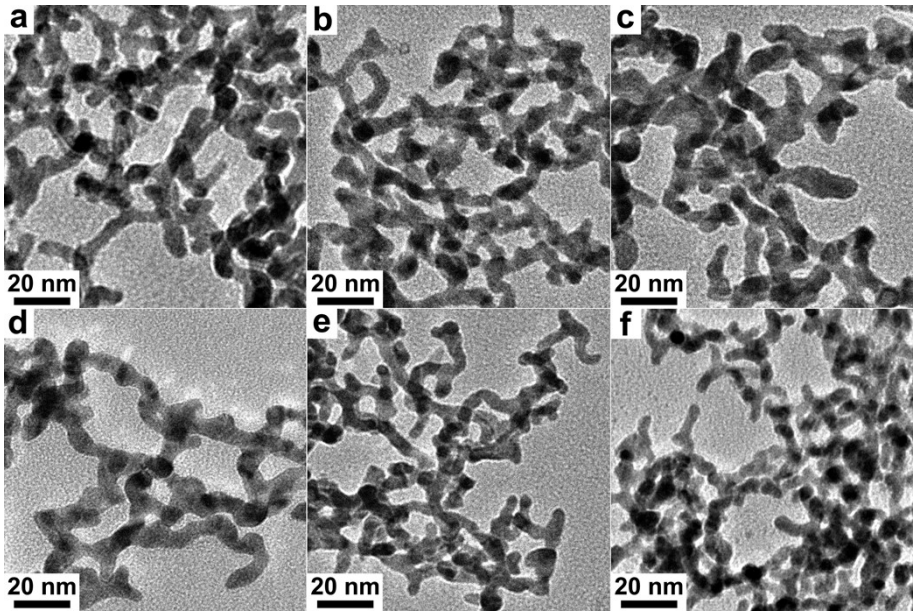

Figure S7. LSV curves (A and D), histograms of η_{10} values (B and E), Tafel slopes (C and F) of a series of S-doped AuPdPt aerogels towards the alkaline HER (0.1 M KOH) and the acidic HER (0.5 M H_2SO_4), respectively, which were prepared under different molar ratios of Pd(II)-to-Pt(IV): 1:9 (a), 2:9 (b), and 3:9 (c).

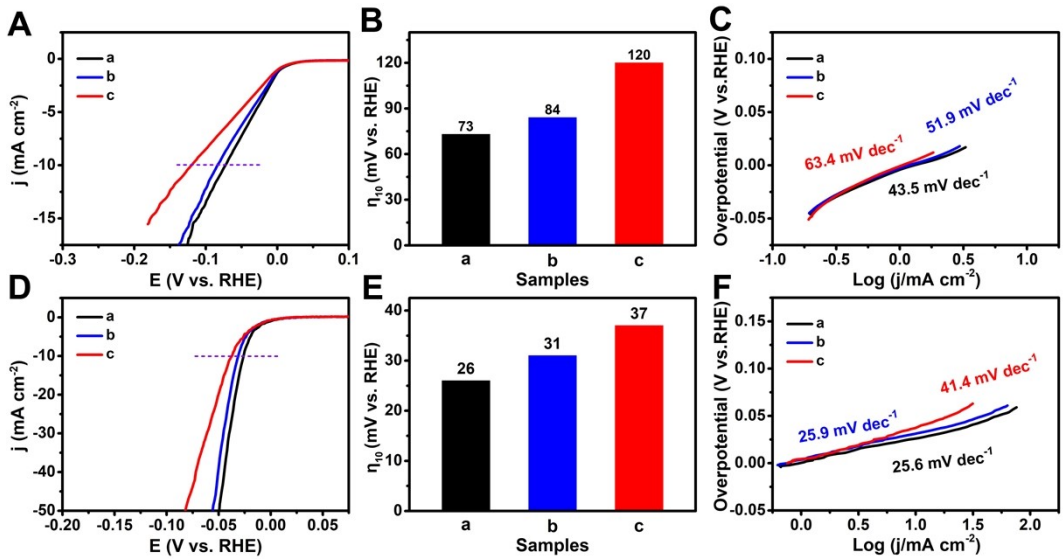

S-doped AuPb aerogels were prepared by secondary $NaBH_4$ reduction, which were used as a template to synthesize S-doped AuPdPt aerogels. These S-doped AuPdPt aerogels were synthesized by the same procedure except that the molar ratios of Pd(II)-to-Pt(IV) precursors were changed from 1:9 to 2:9, and 3:9 accordingly. As shown in **Figure S7A and S7B**, the η_{10} towards the HER in alkaline media of these S-doped AuPdPt aerogels are 73, 84 and 120 mV (*vs.* RHE), respectively. Their Tafel slope are 43.5, 51.9 and 63.4 mV dec^{-1} **(Figure S7C)**. Moreover, as shown in **Figure S7D and S7E**, the η_{10} towards the HER in acidic media of a series of S-doped AuPdPt aerogels are 26, 31 and 37 mV (*vs.* RHE), respectively. And their tafel slope are 25.6, 25.9 and 41.4 mV dec^{-1} **(Figure S7F)**.

Figure S8. LSV curves (A and D), histograms of η_{10} values (B and E), Tafel slopes (C and F) of a series of S-doped AuPdPt aerogels towards the alkaline HER (0.1 M KOH) and the acidic HER (0.5 M H_2SO_4), respectively, which were prepared under different molar ratios of Pd(II)-to-Pt(IV): 1:10 (a), 2:10 (b), and 3:10 (c).

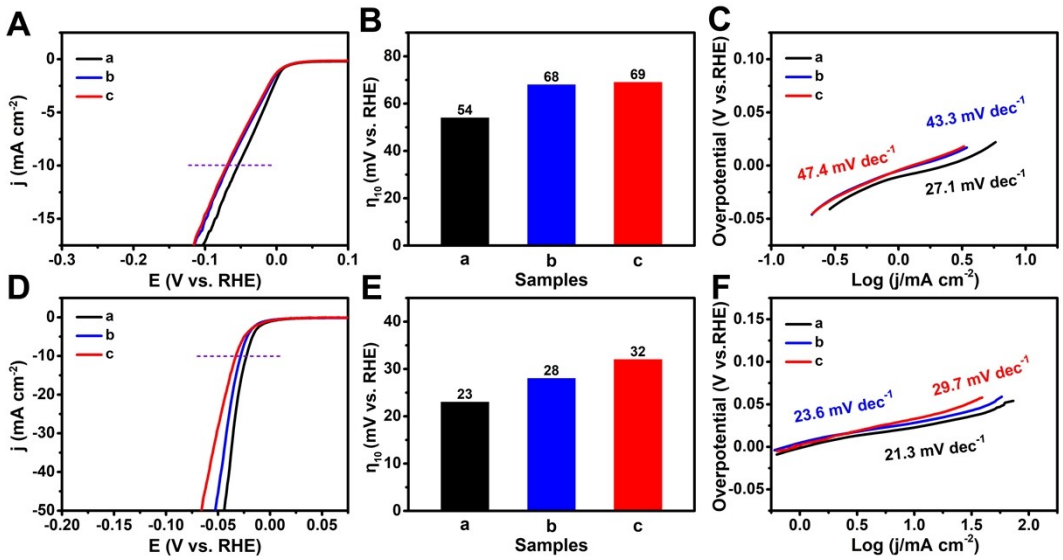

These S-doped AuPdPt aerogels were obtained by the same procedure except that the molar ratios of Pd(II)-to-Pt(IV) precursors were changed from 1:10 to 2:10, and 3:10 accordingly. As shown in **Figure S8A and S8B**, their η_{10} values towards the HER in alkaline media are 54, 68 and 69 mV (*vs.* RHE), respectively. And their Tafel slope are 27.1, 43.3 and 47.4 mV dec^{-1} **(Figure S8C)**. Moreover, as shown in **Figure S8D and S8E**, their η_{10} values towards the HER in acidic media are 23, 28 and 32 mV (*vs.* RHE), respectively. And their Tafel slope are 21.3, 23.6 and 29.7 mV dec^{-1} **(Figure S8F)**.

Figure S9. LSV curves (A and D), histograms of η_{10} values (B and E), Tafel slopes (C and F) of a series of S-doped AuPdPt aerogels towards the alkaline HER (0.1 M KOH) and the acidic HER (0.5 M H_2SO_4), respectively, which were prepared under different molar ratios of Pd(II)-to-Pt(IV): 1:11 (a), 1:12 (b), 1:13 (c), and 1:14 (d).

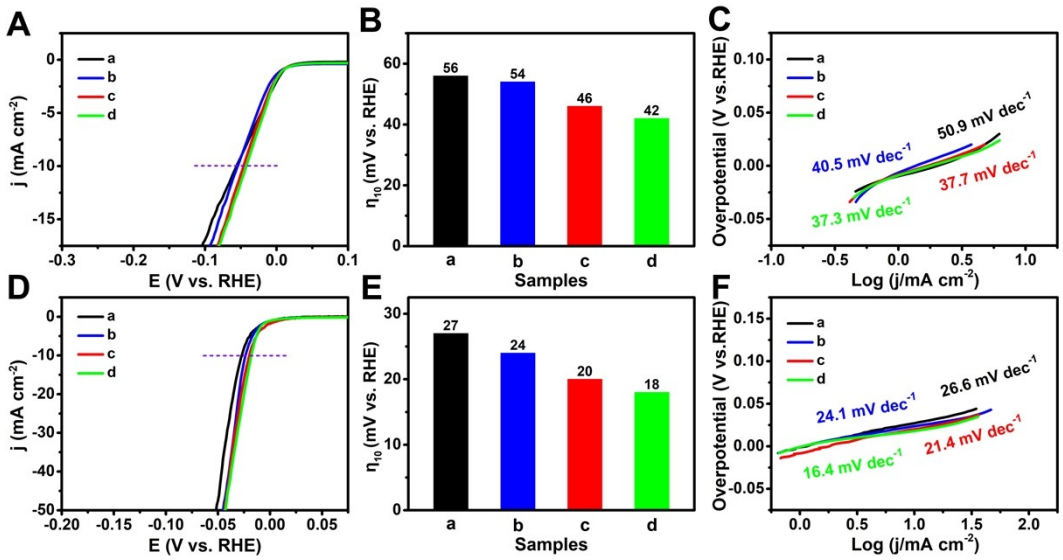

These S-doped AuPdPt aerogels were obtained by the same procedure except that the molar ratios of Pd(II)-to-Pt(IV) precursors were changed from 1:11 to 1:12, 1:13, and 1:14 accordingly. As shown in **Figure S9A and S9B**, their η_{10} values towards the HER in alkaline media are 56, 54, 46 and 42 mV (*vs.* RHE), respectively. And their Tafel slope are 50.9, 40.5, 37.7 and 37.3 mV dec^{-1} **(Figure S9C)**. Moreover, as shown in **Figure S9D and S9E**, their η_{10} values towards the HER in acidic media are 27, 24, 20 and 18 mV (*vs.* RHE), respectively. And their Tafel slope are 26.6, 24.1, 21.4 and 16.4 mV dec^{-1} **(Figure S9F)**.

Figure S10. LSV curves (A and D), histograms of η_{10} values (B and E), Tafel slopes (C and F) of a series of S-doped AuPdPt aerogels towards the alkaline HER (0.1 M KOH) and the acidic HER (0.5 M H_2SO_4), respectively, which were prepared under different molar ratios of Pd(II)-to-Pt(IV): 1:15 (a), 1:16 (b), 1:17 (c), 1:18 (d), and 1:19 (e).

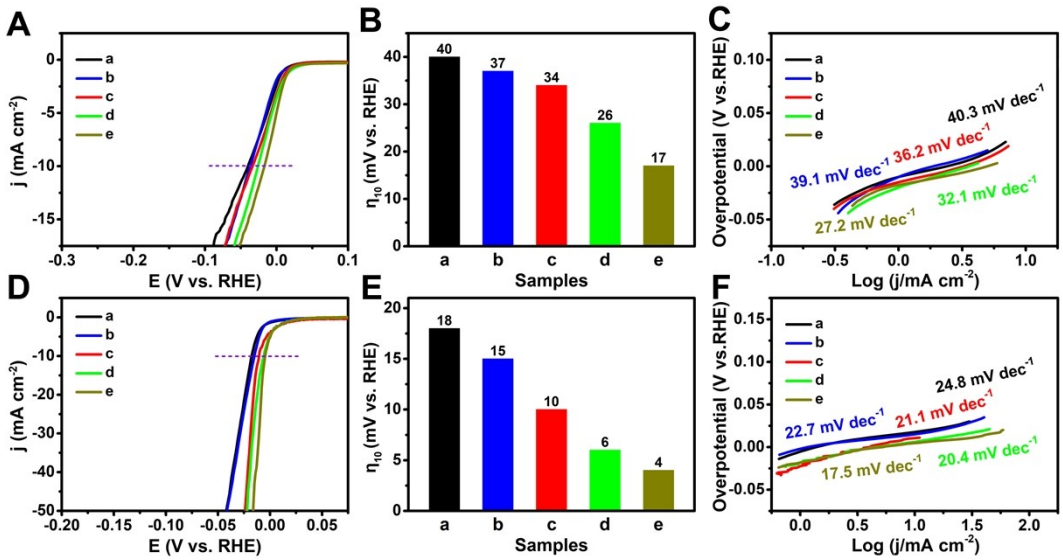

These S-doped AuPdPt aerogels were obtained by the same procedure except that the molar ratios of Pd(II)-to-Pt(IV) precursors were changed from 1:15 to 1:16, 1:17, 1:18, and 1:19 accordingly. As shown in **Figure S10A and S10B**, their η_{10} values towards the HER in alkaline media are 40, 37, 34, 26 and 17 mV (*vs.* RHE), respectively. Their Tafel slope are 40.3, 39.1, 36.2, 32.1 and 27.2 mV dec^{-1} **(Figure S10C)**. Moreover, as shown in **Figure S10D and S10E**, their η_{10} values towards the HER in acidic media are 18, 15, 10, 6 and 4 mV (*vs.* RHE), respectively. And their Tafel slope are 24.8, 22.7, 21.1, 20.4 and 17.5 mV dec^{-1} **(Figure S10F)**.

Figure S11. LSV curves (A and D), histograms of η_{10} values (B and E), Tafel slopes (C and F) of a series of S-doped AuPdPt aerogels towards the alkaline HER (0.1 M KOH) and the acidic HER (0.5 M H_2SO_4), respectively, which were prepared under different molar ratios of Pd(II)-to-Pt(IV): 1:20 (a), 1:21 (b), 1:22 (c), 1:23 (d), 1:24 (e), and 1:25 (f).

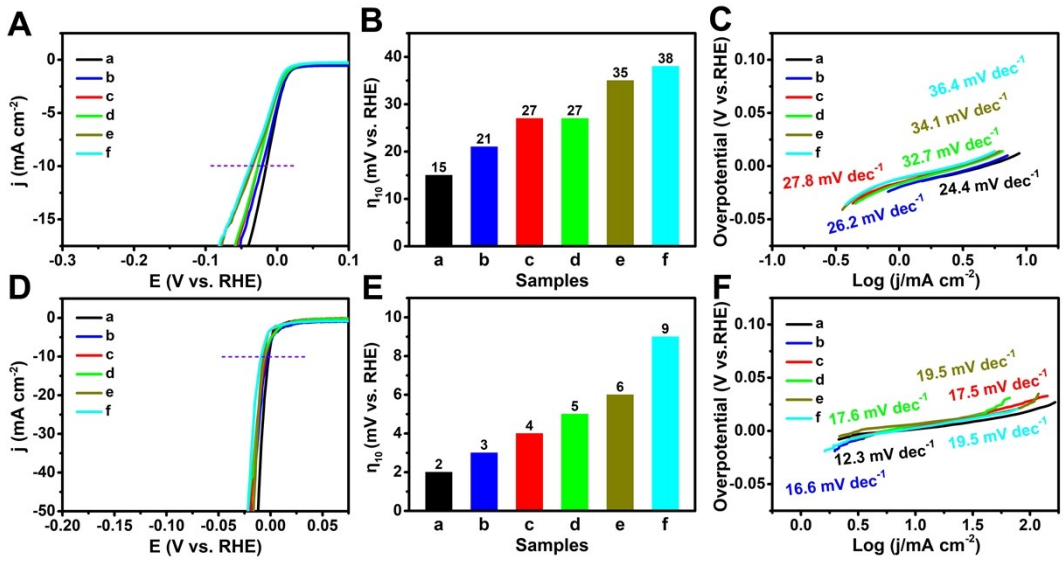

These S-doped AuPdPt aerogels were obtained by the same procedure except that the molar ratios of Pd(II)-to-Pt(IV) precursors were changed from 1:20 to 1:21, 1:22, 1:23, 1:24, and 1:25 accordingly. As shown in **Figure S11A and S11B**, their η_{10} values towards the HER in alkaline media are 15, 21, 27, 27, 35 and 38 mV (*vs.* RHE), respectively. Their Tafel slope are 24.4, 26.2, 27.8, 32.7, 34.1 and 36.4 mV dec^{-1} **(Figure S11C)**. Moreover, as shown in **Figure S11D and S11E**, their η_{10} values towards the HER in acidic media are 2, 3, 4, 5, 6 and 9 mV (*vs.* RHE), respectively. And their Tafel slope are 12.3, 16.6, 17.5, 17.6, 19.5 and 19.5 mV dec^{-1} **(Figure S11F)**. In brief, the molar ratios of Pd(II)-to-Pt(IV) precursors is lower than 1:20, the performance of the S-doped Au/Pd/Pt aerogel towards HER in the alkaline and the acidic media both gradually become worse.

Figure S12. TEM images of a series of S-doped AuPdPt aerogels prepared under different amount of $NaBH_4$ (0.1 M) during the secondary $NaBH_4$ reduction: 50 μL (a and e), 80 μL (b and f), 100 μL (c and g), and 120 μL (d and h). Note that the amount of $NaBH_4$ (0.1 M) during the first reduction was 100 μL.

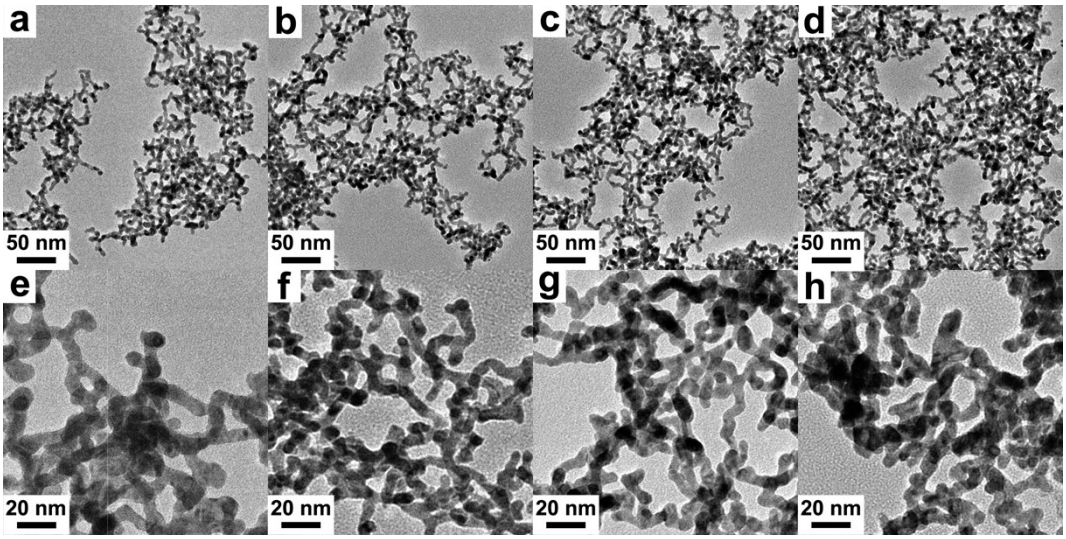

Figure S13. LSV curves (A and D), histograms of η_{10} values (B and E), Tafel slopes (C and F) of a series of S-doped AuPdPt aerogels towards the alkaline HER (0.1 M KOH) and the acidic HER (0.5 M H_2SO_4), respectively, which were prepared under different amount of $NaBH_4$ (0.1 M) during the secondary $NaBH_4$ reduction: 50 μL (a), 80 μL (b), 100 μL (c), 120 μL (d), and 150 μL (e). Note that the amount of $NaBH_4$ (0.1 M) during the first reduction was 100 μL.

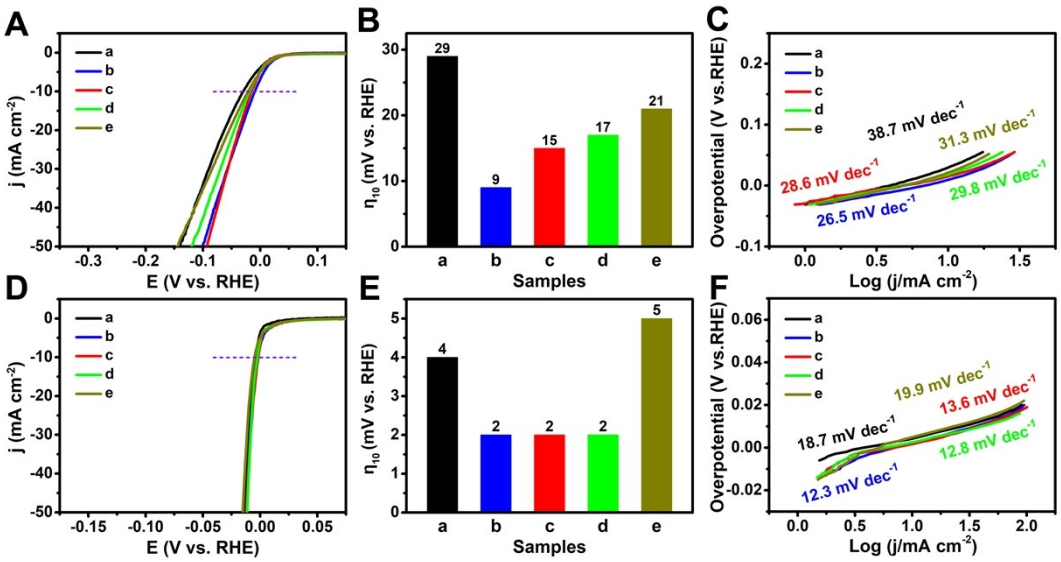

Based on the above experimental results, the molar ratio of Pd(II)-to-Pt(IV) ions was determined to be 1:20, and then the optimal amount of the secondary added $NaBH_4$ was explored. These S-doped AuPdPt aerogels were synthesised by the same procedure except that the amounts of the secondary added $NaBH_4$ were changed from 50 μL to 80 μL, 100 μL, 120 μL, and 150 μL accordingly.

As shown in **Figure S13A and S13B**, their η_{10} values towards the HER in alkaline media are 29, 9, 15, 17 and 21 mV (*vs.* RHE), respectively. Their Tafel slope are 38.7, 26.5, 28.6, 29.8 and 31.3 mV dec^{-1} **(Figure S13C)**. Moreover, as shown in **Figure S13D and S13E**, the η_{10} values towards the HER in acidic media are 4, 2, 2, 2 and 5 mV (*vs.* RHE), respectively. And their Tafel slope are 18.7, 12.3, 13.6, 12.8 and 19.9 mV dec^{-1} **(Figure S13F)**.

Figure S14. High resolution (HR) TEM images of $Au_{81}Pd_2Pt_9$-$S_8^{B4.6A3.4}$ aerogel (a) reported in our previous work, and the as-prepared $S_{6.5}$-doped $Au_{77.6}/Pd_{0.8}/Pt_{15.1}$ aerogel (b) in this work.

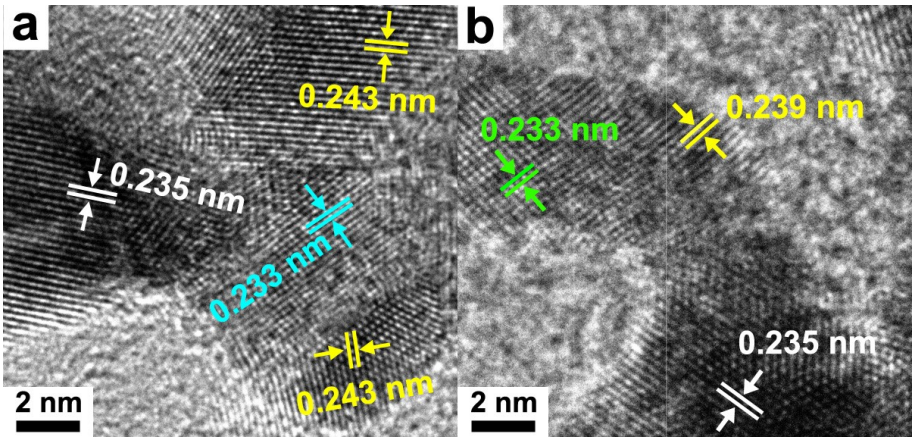

Figure S14a is the HR-TEM image of $Au_{81}Pd_2Pt_9$-$S_8^{B4.6A3.4}$ aerogel reported in our previous work,[1] the lattice spacings of the spherical junctions are about 0.235 nm in average, which is nearly the same as that of the {111} plane of pure Au. In addition, the majority of the lattice spacings at the edge regions of the ligaments is about 0.243 nm in average, which is located between that of the {111} plane of pure Au (0.235 nm) and the {110} plane of pure PtS (0.245 nm); and some lattice spacings at the edge regions of the ligaments are about 0.233 nm, which may be located between that of the {111} plane of pure Au (0.235 nm) and the {111} plane of pure Pd (0.225 nm), Pt (0.227 nm), or between that of the {211} plane of pure PdS_2 (0.232 nm) and the {111} plane of pure Pd (0.225 nm), or pure Pt (0.227 nm). These results indicate that the resulting $Au_{81}Pd_2Pt_9$-$S_8^{B4.6A3.4}$ aerogel may be composed of elemental Au as the main skeleton and alloyed Pd-Pt layers on their outmost surfaces. It is highly possible that Pd-Pt alloyed layers are doped by S^{2-} and S_2^{2-} ligands.

As shown **Figure S14b**, the lattice spacing at the spherical junctions of the ligaments is about 0.235 nm, which is the same as that of the {111} plane of pure Au. The results are rather similar to those S-doped Au-PdPt aerogels reported in our previous work. In contrast, the lattice spacing in other parts of the ligaments is about 0.233 nm, which is located between the {111} plane (0.235 nm) of pure Au and {111} plane (0.227 nm) of pure Pt, and is also rather close to that of Au {111} planes because of the high percentage of Au in them. The result indicates the formation of ultrathin Pt shells. Note that in the outermost edge of the ligaments, some lattice spacing (0.239 nm) belongs to the {110} plane of PtS is observed, indicating the presence of PtS on their outermost surfaces.

Figure S15. EDS spectrum (a) and HAADF-STEM-EDS cross-sectional compositional line profile (b) of the as-prepared $S_{6.5}$-doped $Au_{77.6}/Pd_{0.8}/Pt_{15.1}$ aerogel.

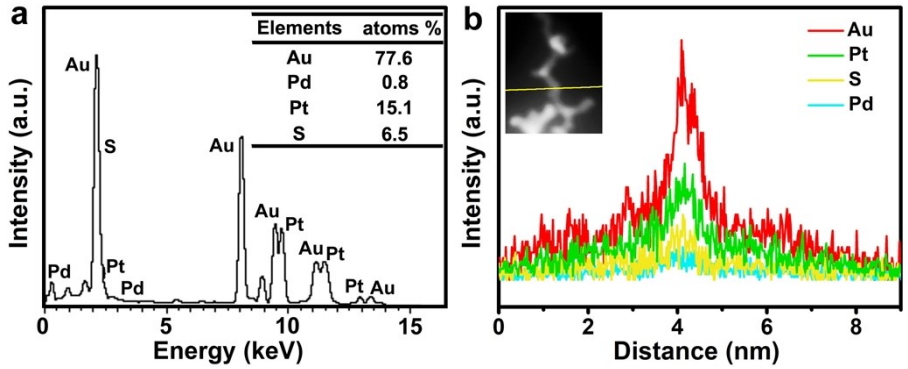

Figure S16. TEM images of non-conformal growth of Pt atoms onto S-doped AuPb aerogel (a and b).

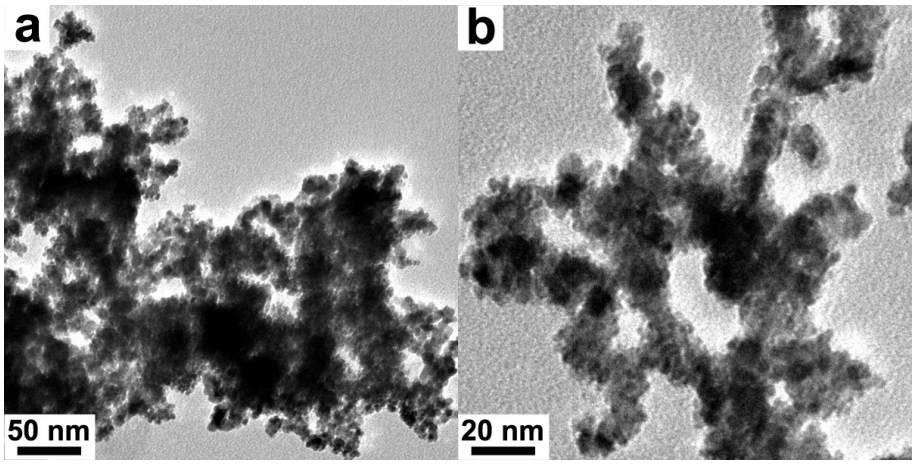

Figure S17. XRD pattern of the as-prepared $S_{6.5}$-doped $Au_{77.6}/Pd_{0.8}/Pt_{15.1}$ aerogel. The standard PDF cards of Au (JCPDS no. 04-0784), Pd (JCPDS no. 46-1043), Pt (JCPDS no. 04-0802), and PtS (JCPDS no. 18-0972) are also provided for better comparison.

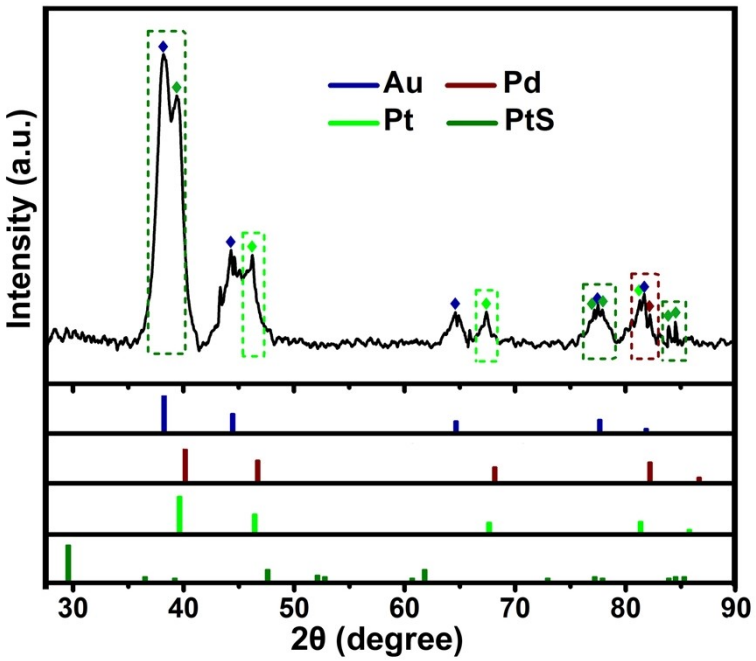

As shown in **Figure S17**, the diffraction peaks of blue rhombus centered at about 38.2°, 44.3°, 64.6°, 77.5° and 81.7° can be attributed to pure Au (JCPDS no. 04-0784), because of the high percentage of Au in them. Moreover, the diffraction peaks of green rhombus in green rectangle (centered at about 46.4°, 67.4° and 81.3°), olive green rhombus in olive rectangle (centered at about 39.3°, 77.2°, 77.9°, 83.9° and 84.5°) are observed in the XRD patterns of the as-prepared $S_{6.5}$-doped $Au_{77.6}/Pd_{0.8}/Pt_{15.1}$ aerogel, which are mainly assigned to Pt and PtS, respectively, on the basis of the corresponding standard PDF cards (JCPDS no. 04-0802, and no. 18-0972). Note that only one diffraction peak belonging to Pd (burgundy rhombus in burgundy rectangle, centered at about 82.1°) is observed in the XRD patterns, on the basis of the corresponding standard PDF cards (JCPDS no. 46-1043), indicating the low content of Pd in the as-prepared $S_{6.5}$-doped $Au_{77.6}/Pd_{0.8}/Pt_{15.1}$ aerogel.

Figure S18. Projection figure of $S_{6.5}$-doped $Au_{77.6}/Pd_{0.8}/Pt_{15.1}$ aerogel under TEM light.

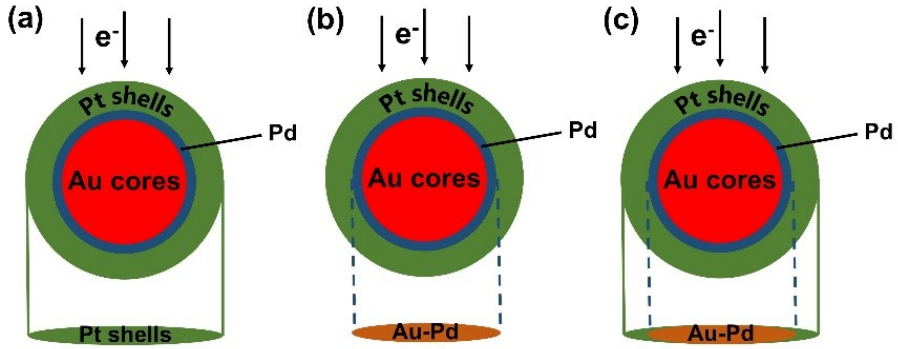

Figure S19. CO stripping voltammograms of $Au_{81}Pd_2Pt_9$-$S_8^{B4.6A3.4}$ aerogel (a) reported in our previous work, the as-prepared $S_{6.5}$-doped $Au_{77.6}/Pd_{0.8}/Pt_{15.1}$ aerogel (b) in this work, and commercial Pt/C catalysts (c). All of curves were measured in a N_2-saturated 0.5 M H_2SO_4 solution with a scan rate of 50 mV s^{-1}.

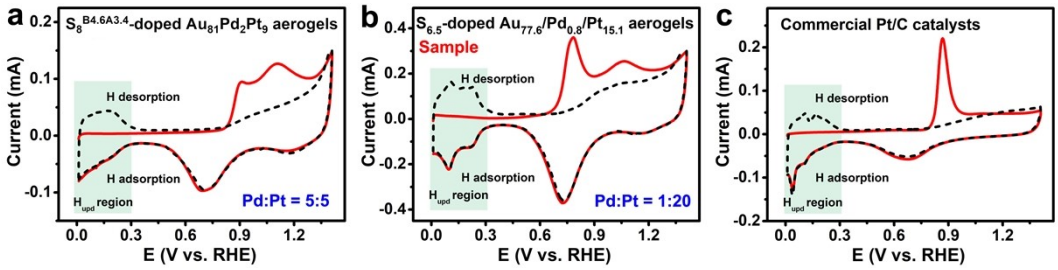

As shown in **Figure S19a**, the $Au_{81}Pd_2Pt_9$-$S_8^{B4.6A3.4}$ aerogel exhibited a weaker and less obvious low-potential CO stripping peak previously reported in our group. [1] Moreover, their H_{upd} (hydrogen adsorption desorption) regions within the potential range from 0 to 0.4 V (*vs.* RHE) were more rounded, whereas $S_{6.5}$-doped $Au_{77.6}/Pd_{0.8}/Pt_{15.1}$ aerogel showed a stronger and obvious low-potential CO stripping peak, and their H_{upd} regions were similar in shape to that of commercial Pt/C catalysts, both of which were sharper. These results further confirm that the $S_{6.5}$-doped $Au_{77.6}/Pd_{0.8}/Pt_{15.1}$ aerogel has a Pt-rich surface, rather than a Pd-Pt alloyed surface.

The electrochemical active surface areas (ECSA) of the samples are calculated based on the equation:

$$ECSA_{CO} = \frac{Q}{mC}$$

Where Q is the charge in the CO adsorption region, m is the Pd/Pt mass loading on the electrode, and C is the charge required for monolayer adsorption of CO on Pd/Pt surface (420 μC cm^{-2}).

The calculated $ECSA_{CO}$ values of commercial Pd/C catalysts, commercial Pt/C catalysts, $Au_{81}Pd_2Pt_9$-$S_8^{B4.6A3.4}$ aerogel, and the as-prepared $S_{6.5}$-doped $Au_{77.6}/Pd_{0.8}/Pt_{15.1}$ aerogel are 59.45 m^2 g_{Pd}^{-1}, 63.96 m^2 g_{Pt}^{-1}, 162.16 m^2 g_{Pd+Pt}^{-1}, and 178.55 m^2 g_{Pd+Pt}^{-1}, respectively. Compared with commercial Pd/C catalysts and commercial Pt/C catalysts, the larger ECSA values of the as-prepared $S_{6.5}$-doped $Au_{77.6}/Pd_{0.8}/Pt_{15.1}$ aerogel indicate that there are more active sites on their surfaces.

Figure S20. CO stripping voltammograms of a series of S-doped AuPdPt aerogel prepared under different molar ratios of Pd(II)-to-Pt(IV): 1:10 (a), 1:13 (b), 1:17 (c), and 1:20 (d).

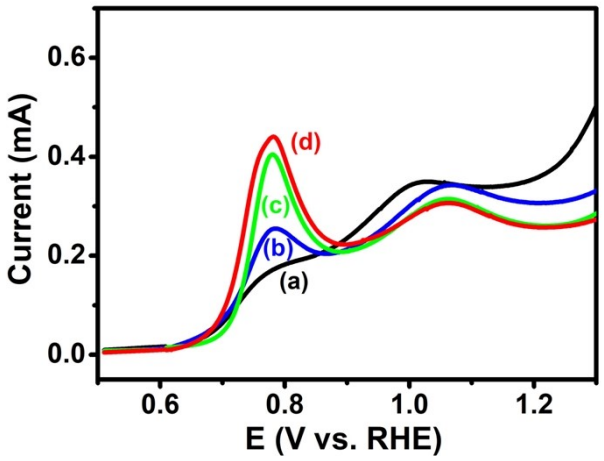

With the increasing Pt content, the center positions of the low-potential CO stripping peaks of these S-doped AuPdPt aerogel gradually become obvious **(Figure S20)**. And their peak positions are located at 0.779 V, 0.785 V, 0.780 V, 0.781 V, respectively, which are closer to that (0.869 V) of commercial Pt/C catalysts. These results indicate the gradual formation of a Pt-rich surfaces on them.

Figure S21. CO stripping voltammograms of a series of S-doped AuPdPt aerogel prepared under different molar ratios of Pd(II)-to-Pt(IV): 1:10 (a), 1:13 (b), 1:17 (c). All of curves were measured in a N_2-saturated 0.5 M H_2SO_4 solution with a scan rate of 50 mV s^{-1}.

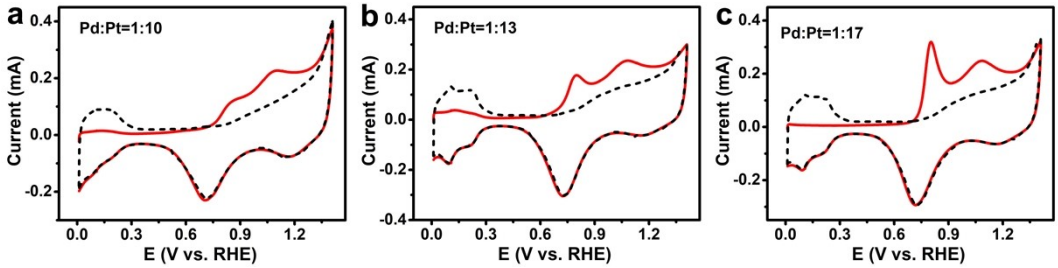

The calculated $ECSA_{CO}$ values of these S-doped AuPdPt aerogel (a, b and c) are 113.21, 143.25 and 165.41 m^2 g_{Pd+Pt}^{-1}.

Figure S22. CO stripping voltammograms of commercial Pt/C catalysts (a) and the as-prepared $S_{6.5}$-doped $Au_{77.6}/Pd_{0.8}/Pt_{15.1}$ aerogel (b), which were measured in a N_2-saturated 0.1 M KOH solution with a scan rate of 50 mV s^{-1}.

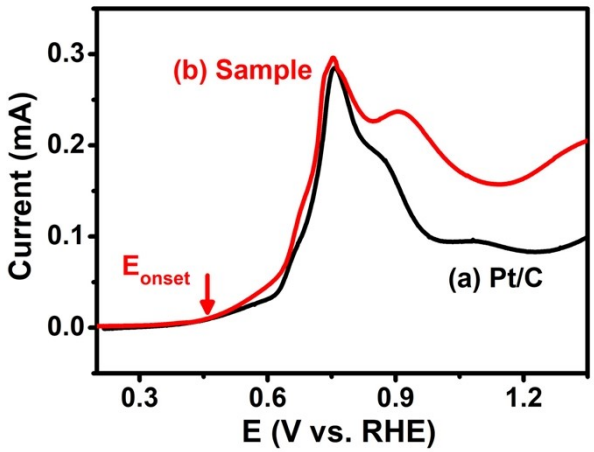

As shown in **Figure S22**, the CO stripping peaks of the as-prepared $S_{6.5}$-doped $Au_{77.6}/Pd_{0.8}/Pt_{15.1}$ aerogel is composed of two peaks, which are located at 0.752 V and 0.904 V (*vs.* RHE). And the one located at about 0.752 V is named as the low-potential CO stripping peak. The low-potential CO stripping peak is closer to that (0.747 V) of commercial Pt/C catalysts, and their shapes are also similar. Moreover, the E_{onset} of the as-prepared $S_{6.5}$-doped $Au_{77.6}/Pd_{0.8}/Pt_{15.1}$ aerogel (0.415 V) in alkaline media is also negative than that (0.454 V) of commercial Pt/C catalysts, indicating that its adsorption ability to oxygen-containing intermediates (such as CO, *OH) becomes weaker.

Figure S23. EDS spectra of $S_{5.9}$-doped $Au_{79.2}/Pd_{0.8}/Pt_{14.1}$ aerogel (a), $S_{6.1}$-doped $Au_{78.2}/Pd_{0.8}/Pt_{14.9}$ aerogel (b), the as-prepared $S_{6.5}$-doped $Au_{77.6}/Pd_{0.8}/Pt_{15.1}$ aerogel (c), and $S_{7.2}$-doped $Au_{76.2}/Pd_{0.8}/Pt_{15.8}$ aerogel (d). The templates of S-doped AuPb aerogel used for synthesis of these S-doped AuPdPt aerogel were prepared under different amount of $NaBH_4$ (0.1 M) during the secondary reduction: (b) 120 μL, (c) 100 μL, (d) 80 μL, and (e) 50 μL. Note that the amount of $NaBH_4$ (0.1 M) during the first reduction was 100 μL.

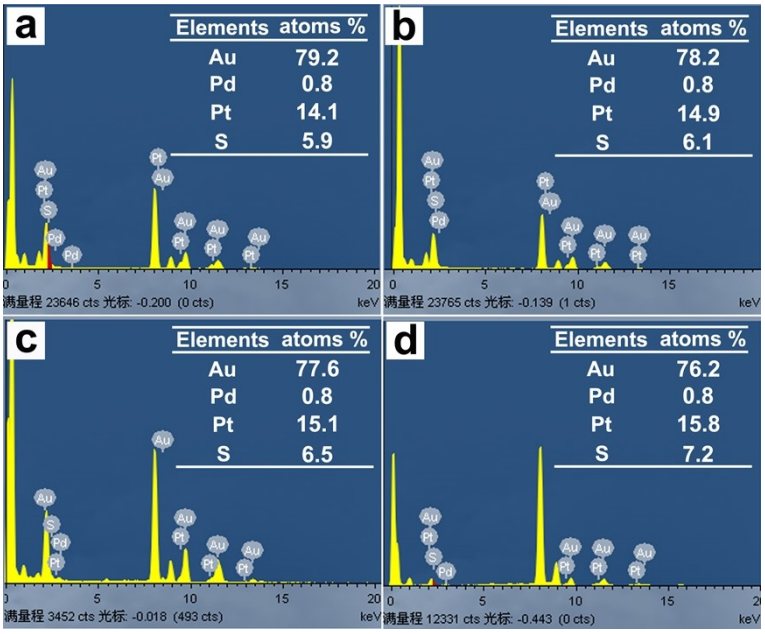

Figure S24. XPS spectra of O 1s orbitals of $S_{5.9}$-doped $Au_{79.2}/Pd_{0.8}/Pt_{14.1}$ aerogel (a), $S_{6.1}$-doped $Au_{78.2}/Pd_{0.8}/Pt_{14.9}$ aerogel (b), the as-prepared $S_{6.5}$-doped $Au_{77.6}/Pd_{0.8}/Pt_{15.1}$ aerogel (c), and $S_{7.2}$-doped $Au_{76.2}/Pd_{0.8}/Pt_{15.8}$ aerogel (d).

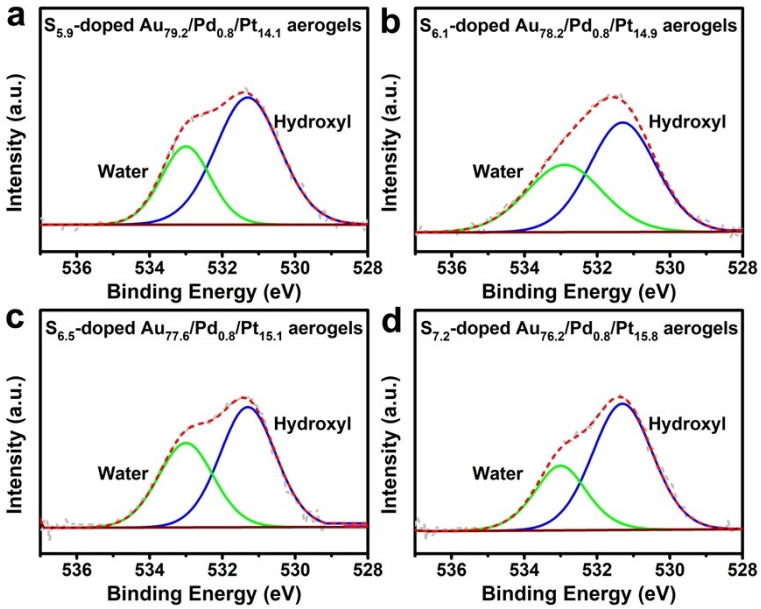

As shown in **Figure S24**, BEs of O 1s signal of these four S-doped AuPdPt aerogels (including $S_{5.9}$-doped $Au_{79.2}/Pd_{0.8}/Pt_{14.1}$ aerogel, the as-prepared $S_{6.5}$-doped $Au_{78.2}/Pd_{0.8}/Pt_{14.9}$ aerogel, $S_{6.5}$-doped $Au_{77.6}/Pd_{0.8}/Pt_{15.1}$ aerogel, $S_{7.2}$-doped $Au_{76.2}/Pd_{0.8}/Pt_{15.8}$ aerogel) are all about 531.3 eV and 533.0 eV, which can be ascribed to the surface hydroxyl groups and adsorbed water, respectively, instead of the lattice oxygen. [2-4] Thus, the results indicate that the species of Pt(II) and Pd(II) are in these S-doped AuPdPt aerogels are mainly combined with elemental S to form sulfides, rather than PtO and PdO.

Figure S25. XPS spectra of Pd 3d orbitals of pure Pd NPs (a), XPS spectra of Au 4d, Pd 3d, Pt 4d orbitals of $S_{5.9}$-doped $Au_{79.2}/Pd_{0.8}/Pt_{14.1}$ aerogel (b), $S_{6.1}$-doped $Au_{78.2}/Pd_{0.8}/Pt_{14.9}$ aerogel (c), the as-prepared $S_{6.5}$-doped $Au_{77.6}/Pd_{0.8}/Pt_{15.1}$ aerogel (d), and $S_{7.2}$-doped $Au_{76.2}/Pd_{0.8}/Pt_{15.8}$ aerogel (e).

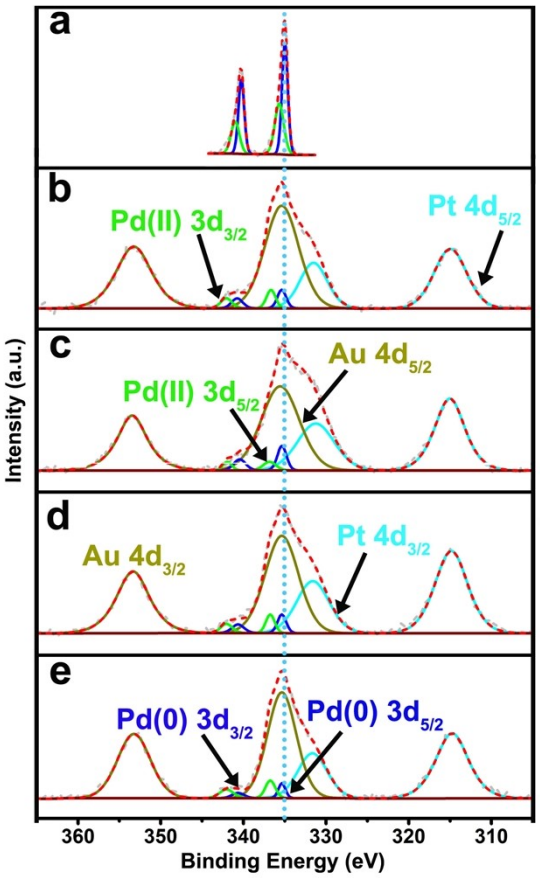

As shown in **Figure S25**, the binding energies (BEs) of Pt $4d_{5/2}$ and Pt $4d_{3/2}$ are 314.8 eV and 331.4 eV while those of Au $4d_{5/2}$ and Au $4d_{3/2}$ are 335.2 eV and 353.2 eV. One can see taht the BEs of the Au 4d orbitals and the Pt 4d orbitals of these S-doped AuPdPt aerogelss are almost the same, but there is a slight difference in their BEs of Pd 3d orbitals. Specifically, the BEs of the Pd(0) $3d_{5/2}$ and Pd(0) $3d_{3/2}$ of Pd(0) species in the samples (b to e) are 335.37 and 340.67 eV **(Figure S25b)**, 335.36 and 340.66 eV **(Figure S25c)**, 335.35 and 340.65 eV **(Figure S25d)**, 335.37 and 340.67 eV **(Figure S25e)**, respectively. Moreover, the BEs of the Pd(II) $3d_{5/2}$ and Pd(II) $3d_{3/2}$ of Pd(II) species in the samples (b to e) are 336.77 and 342.07 eV **(Figure S25b)**, 336.76 and 342.06 eV **(Figure S25c)**, 336.75 and 342.05 eV **(Figure S25d)**, 336.77 and 342.07 eV **(Figure S25e)**, respectively.

Figure S26. XPS spectra of S 2p orbitals of $S_{5.9}$-doped $Au_{79.2}/Pd_{0.8}/Pt_{14.1}$ aerogel (a), $S_{6.1}$-doped $Au_{78.2}/Pd_{0.8}/Pt_{14.9}$ aerogel (b), and $S_{7.2}$-doped $Au_{76.2}/Pd_{0.8}/Pt_{15.8}$ aerogel (c).

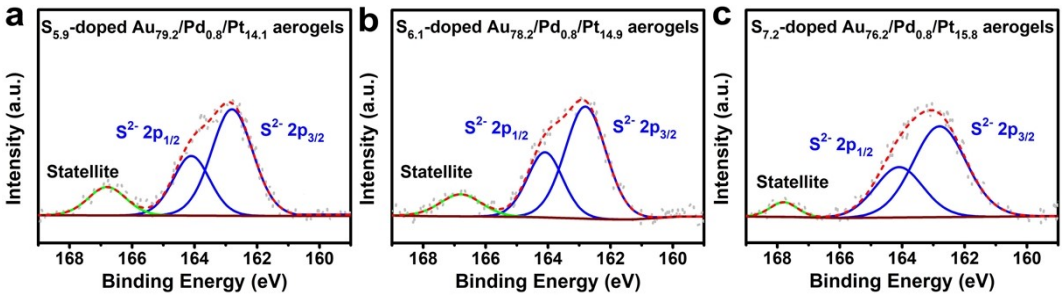

Figure S27. XPS spectra of Au 4f orbitals of pure Au NPs (a) and $S_{5.9}$-doped $Au_{79.2}/Pd_{0.8}/Pt_{14.1}$ aerogel (b), $S_{6.1}$-doped $Au_{78.2}/Pd_{0.8}/Pt_{14.9}$ aerogel (c), the as-prepared $S_{6.5}$-doped $Au_{77.6}/Pd_{0.8}/Pt_{15.1}$ aerogel (d), and $S_{7.2}$-doped $Au_{76.2}/Pd_{0.8}/Pt_{15.8}$ aerogel (e).

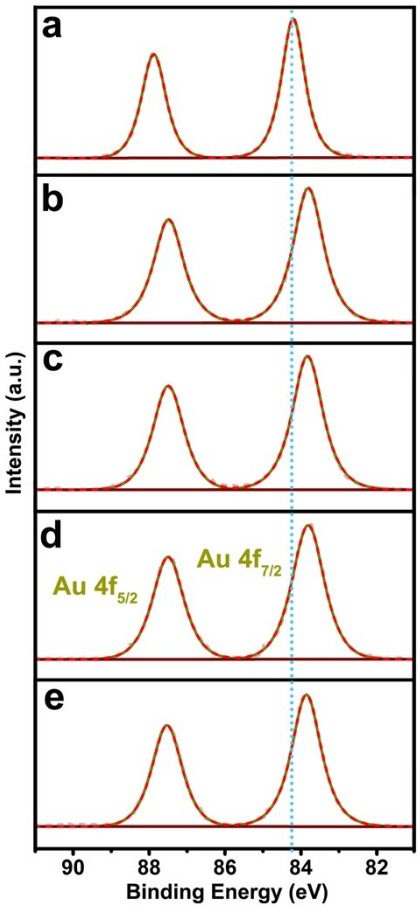

Figure S28. SERS spectra of S-doped AuPb aerogel (a), S-doped AuPd aerogel (b), $Au_{81}Pd_2Pt_9$-$S_8^{B4.6A3.4}$ aerogel (c) reported in our previous work, the as-prepared $S_{6.5}$-doped $Au_{77.6}/Pd_{0.8}/Pt_{15.1}$ aerogel (d) in this work, S-doped AuPdPt aerogel (e). The amount of Pd(II) ions used in S-doped AuPd aerogel is set as 1. And the molar ratios of Pd(II)-to-Pt(IV) ions used in samples (c, d and e) are 5:5, 1:20 and 1:25, respectively. The excitation laser wave length, the laser power and the exposure time is 633 nm, 0.05 W, and 10 s, respectively.

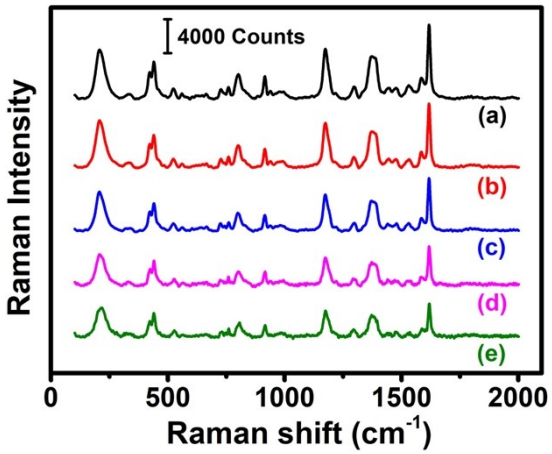

The same volume of dispersion containing these S-doped AuPdPt aerogels were mixed with the probe of crystalline violet (CV, 10^{-6} M). As shown in **Figure S28**, the signal intensities of the Raman characteristic peaks (located at 207, 1170, and 1617 cm^{-1}) of CVs in the surface enhanced Raman scattering (SERS) spectra of the samples (a to e) is gradually weakened with the increasing metal amounts (Pd + Pt) grown on the surfaces of S-doped AuPb aerogels. The molar amount of Pd(II) ions is set as 1, which is 1% of the Au molar amount in S-doped AuPb aerogels. However, the presence of SERS signal of CVs indicates that the SPR effect of Au cores in these samples still can act on their outermost surfaces, especially when the metal amounts (Pd + Pt) reached 26 (1:25). And the presence of the atomic-scale Au-Pd-Pt diffuse interface still can facilitate the electron transfer between Au cores and Pt shells.

Figure S29. The enlarged coupling areas (green areas in a, b and c) between Au $4d_{5/2}$ and Pt $4d_{3/2}$ orbitals after the integrating processing of $S_{5.9}$-doped $Au_{79.2}/Pd_{0.8}/Pt_{14.1}$ aerogel (a), $S_{6.1}$-doped $Au_{78.2}/Pd_{0.8}/Pt_{14.9}$ aerogel (b), and $S_{7.2}$-doped $Au_{76.2}/Pd_{0.8}/Pt_{15.8}$ aerogel (c).

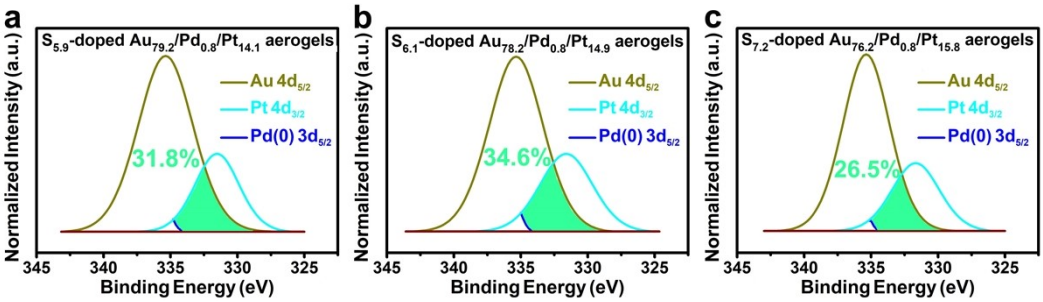

Figure S30. EIS spectra of commercial Pt/C catalysts (a) and the as-prepared $S_{6.5}$-doped $Au_{77.6}/Pd_{0.8}/Pt_{15.1}$ aerogel (b).

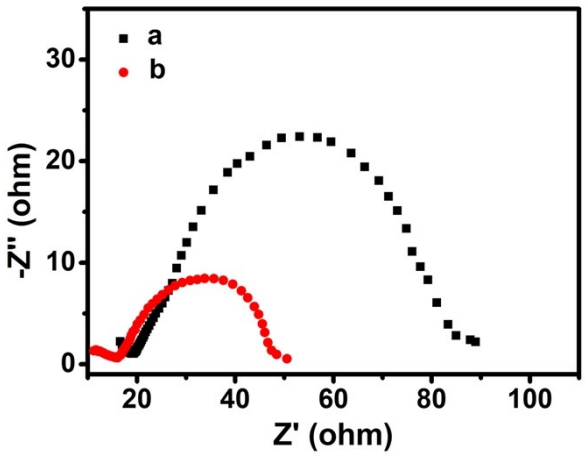

Figure S31. TOF curves (A) and histograms (B) of TOF values at -0.05 V of commercial Pt/C catalysts (a) and the as-prepared $S_{6.5}$-doped $Au_{77.6}/Pd_{0.8}/Pt_{15.1}$ aerogel (b).

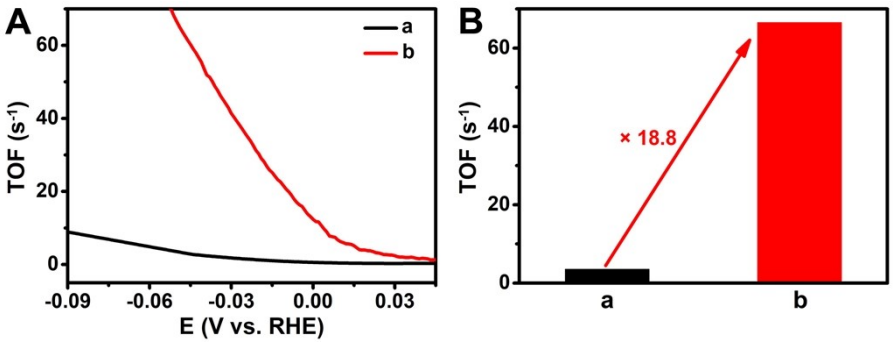

The turnover frequency (TOF) is obtained according to the following equation:

$$TOF = \frac{I}{2Fn}$$

where I is the current density, F is the faraday constant (96485 C mol^{-1}), and n is the number of moles of Pt.

Figure S32. LSV curves of commercial Pt/C catalysts towards the alkaline HER before and after the ADT tests of 5k cycles.

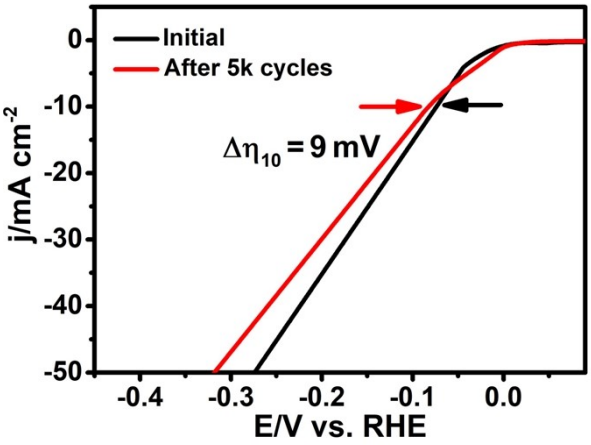

Figure S33. (A and C) Tafel plots of the as-prepared $S_{6.5}$-doped $Au_{77.6}/Pd_{0.8}/Pt_{15.1}$ aerogel (A) and commercial Pt/C catalysts (C) towards the alkaline HER before and after the ADT tests of 5k cycles; (B and D) Histograms of mass activity (at -0.05 V) and current density (at -0.07 V) of the as-prepared $S_{6.5}$-doped $Au_{77.6}/Pd_{0.8}/Pt_{15.1}$ aerogel (B) and commercial Pt/C catalysts (D) towards the alkaline HER before (a) and after (b) the ADT tests.

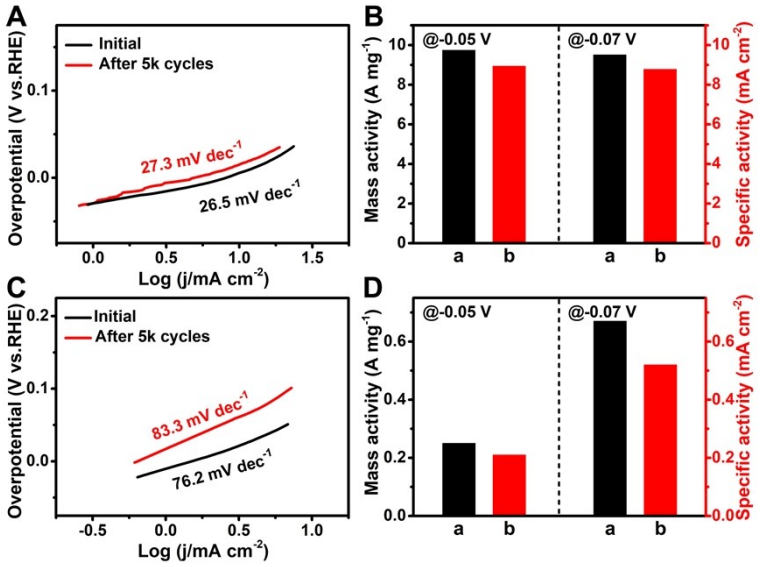

As shown in **Figure S33A**, the as-prepared $S_{6.5}$-doped $Au_{77.6}/Pd_{0.8}/Pt_{15.1}$ aerogel show a negligible change in their Tafel plot before and after the ADT tests of 5k cycles and so do their Tafel slopes. In contrast, commercial Pt/C catalysts display an obvious change in their Tafel plots and their Tafel slopes were increased from 76.2 to 83.3 mV dec^{-1} **(Figure S33C)**. Moreover, the mass activity (at -0.05 V) of the as-prepared $S_{6.5}$-doped $Au_{77.6}/Pd_{0.8}/Pt_{15.1}$ aerogel was 91.8% of the initial one before and after the ADT test of 5k cycles, while that of commercial Pt/C catalysts was only 84.0% of the initial one **(Figure S33B and D)**. Furthermore, the current density (at -0.07 V) of the as-prepared $S_{6.5}$-doped $Au_{77.6}/Pd_{0.8}/Pt_{15.1}$ aerogel was 92.3% of the initial one after the ADT tests of 5k cycles while that of commercial Pt/C catalysts was 77.6% of the initial one **(Figure S33B and D)**. Therefore, the long-term stability of the as-prepared $S_{6.5}$-doped $Au_{77.6}/Pd_{0.8}/Pt_{15.1}$ aerogel towards the HER in alkaline media is much better than that of commercial Pt/C catalysts.

Figure S34. TEM image of the as-prepared $S_{6.5}$-doped $Au_{77.6}/Pd_{0.8}/Pt_{15.1}$ aerogel towards (a) the alkaline and (b) the acidic HER after the ADT test.

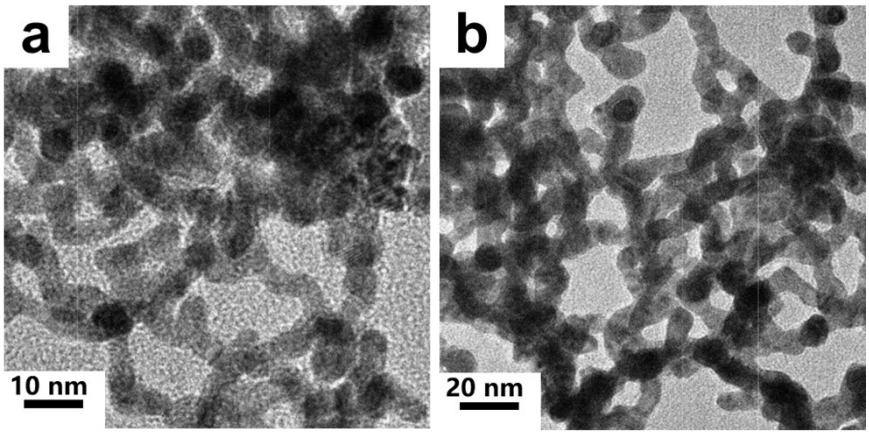

By compared with TEM image of the as-prepared $S_{6.5}$-doped $Au_{77.6}/Pd_{0.8}/Pt_{15.1}$ aerogel before (**Fig. 1a** and **1b**), one can clearly see that the diameter of the ligands in the as-prepared $S_{6.5}$-doped $Au_{77.6}/Pd_{0.8}/Pt_{15.1}$ aerogel after the ADT test (**Figure S34**) is nearly same to that before the ADT test. The result further demonstrates that the as-prepared $S_{6.5}$-doped $Au_{77.6}/Pd_{0.8}/Pt_{15.1}$ aerogel has an excellent stability towards the alkaline HER and the acidic HER.

Figure S35. LSV curves (A and C) and corresponding Tafel plots (B and D) of the as-prepared $S_{6.5}$-doped $Au_{77.6}/Pd_{0.8}/Pt_{15.1}$ aerogel (A) in this work and $Au_{81}Pd_2Pt_9$-$S_8B^{4.6A3.4}$ aerogel (C) in our previous work before (black line) and after (red line) the ADT tests of 5k cycles, which were measured in alkaline media.

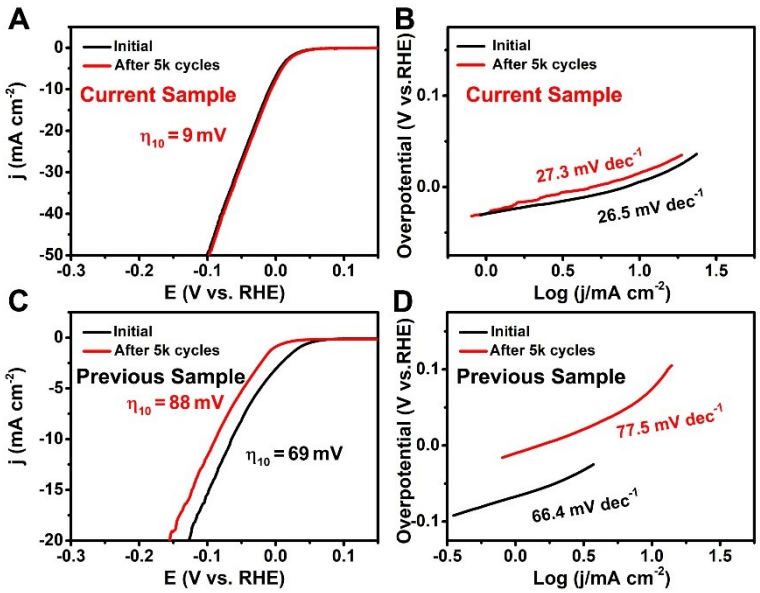

As shown in **Figure S35A**, the change in LSV curves of the as-prepared $S_{6.5}$-doped $Au_{77.6}/Pd_{0.8}/Pt_{15.1}$ aerogel before and after the ADT tests of 5k cycles is slightly changed (9 mV) while that of $Au_{81}Pd_2Pt_9$-$S_8B^{4.6A3.4}$ aerogel is obviously changed (19 mV, from 69 to 88 mV). In additiion, the change in the Tafel plot of of the as-prepared $S_{6.5}$-doped $Au_{77.6}/Pd_{0.8}/Pt_{15.1}$ aerogel before and after the ADT tests of 5k cycles is slightly changed from 26.5 to 27.3 mV dec^{-1} (**Figure S35B)** while the Tafel slopes of that of $Au_{81}Pd_2Pt_9$-$S_8B^{4.6A3.4}$ aerogel were obviuosly changed from 66.4 to 77.5 mV dec^{-1} **(Figure S35C and D)**. Therefore, the catalytic activity and the long-term stability of the as-prepared $S_{6.5}$-doped $Au_{77.6}/Pd_{0.8}/Pt_{15.1}$ aerogel in this work towards the HER in allakaline media is a much better than those of the $Au_{81}Pd_2Pt_9$-$S_8B^{4.6A3.4}$ aerogel reported in our previous work.

Figure S36. EIS spectra of commercial Pt/C catalysts (a) and the as-prepared $S_{6.5}$-doped $Au_{77.6}/Pd_{0.8}/Pt_{15.1}$ aerogel (b).

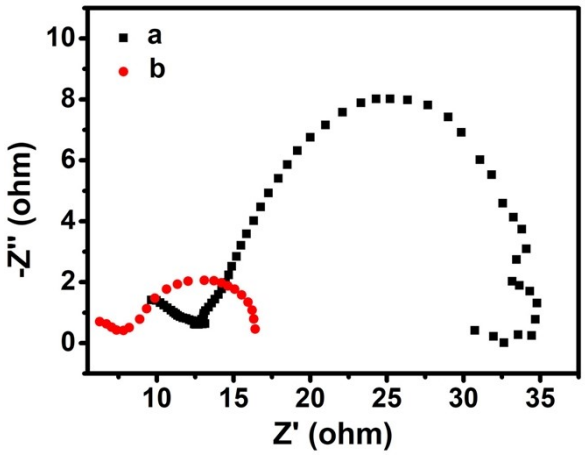

Figure S37. TOF curves (A) and histograms (B) of TOF values at -0.05 V of commercial Pt/C catalysts (a) and the as-prepared $S_{6.5}$-doped $Au_{77.6}/Pd_{0.8}/Pt_{15.1}$ aerogel (b).

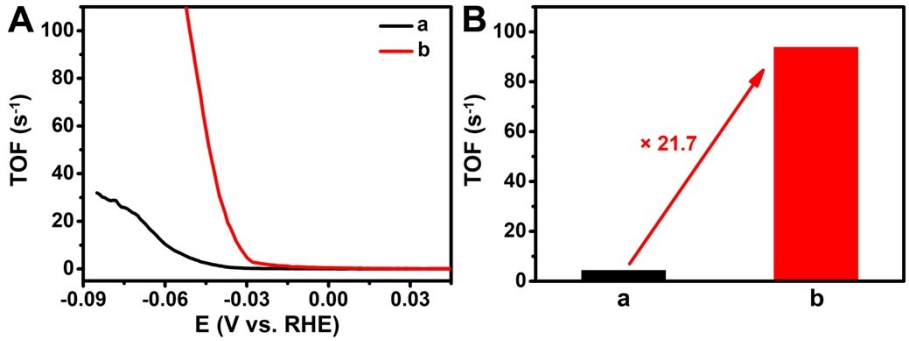

Figure S38. LSV curves of commercial Pt/C catalysts towards the acidic HER before and after the ADT tests of 5k cycles.

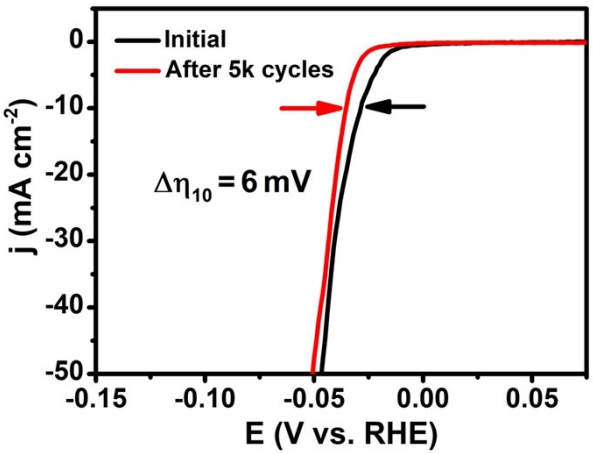

Figure S39. LSV curves (A and C) and corresponding Tafel plots (B and D) of the as-prepared $S_{6.5}$-doped $Au_{77.6}/Pd_{0.8}/Pt_{15.1}$ aerogel (A) in this work and $Au_{81}Pd_2Pt_9$-$S_8B^{4.6A3.4}$ aerogel (C) in our previous work before (black line) and after (red line) the ADT tests of 5k cycles, which were measured in acidic media.

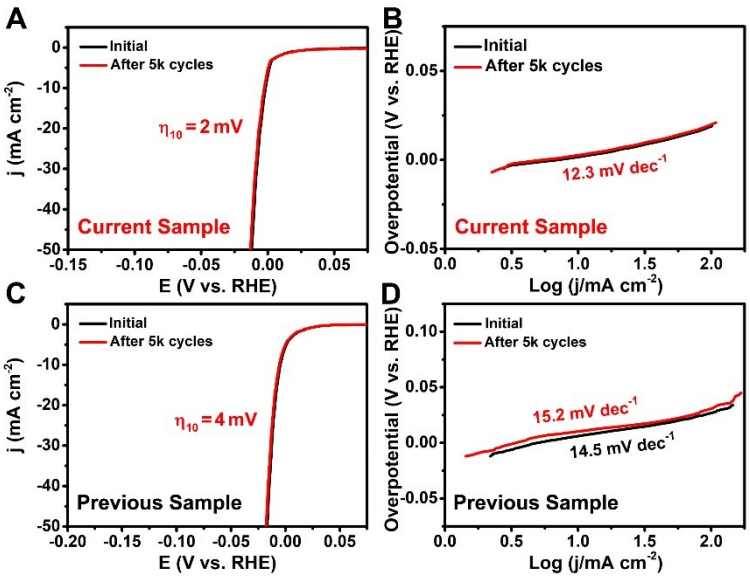

As shown in **Figure S39A and S39B**, the as-prepared $S_{6.5}$-doped $Au_{77.6}/Pd_{0.8}/Pt_{15.1}$ aerogel show a negligible change (2 mV) in their LSV curves before and after the ADT tests of 5k cycles in acidic media and so do their Tafel slopes. In contrast, the change in the LSVs of the $Au_{81}Pd_2Pt_9$-$S_8B^{4.6A3.4}$ aerogel reported in our previous work is also negligible (4 mV) before and after the ADT tests of 5k cycles **(Figure S39C).** In addition, their Tafel slopes were also slightly changed from 14.5 to 15.2 mV dec^{-1} **(Figure S39D)**. Therefore, the catalytic activity and the long-term stability of the as-prepared $S_{6.5}$-doped $Au_{77.6}/Pd_{0.8}/Pt_{15.1}$ aerogel in this work towards the HER in acidic media is a little better than those of the $Au_{81}Pd_2Pt_9$-$S_8B^{4.6A3.4}$ aerogel reported in our previous work.

Figure S40. Tafel plots (A and C) of the as-prepared $S_{6.5}$-doped $Au_{77.6}/Pd_{0.8}/Pt_{15.1}$ aerogel (A) and commercial Pt/C catalysts (C) towards the acidic HER before and after the ADT tests of 5k cycles; Histograms of mass activity (at -0.05 V) and current density (at -0.07 V) (B and D) of the as-prepared $S_{6.5}$-doped $Au_{77.6}/Pd_{0.8}/Pt_{15.1}$ aerogel (B) and commercial Pt/C catalysts (D) towards the acidic HER before (a) and after (b) the ADT tests of 5k cycles.

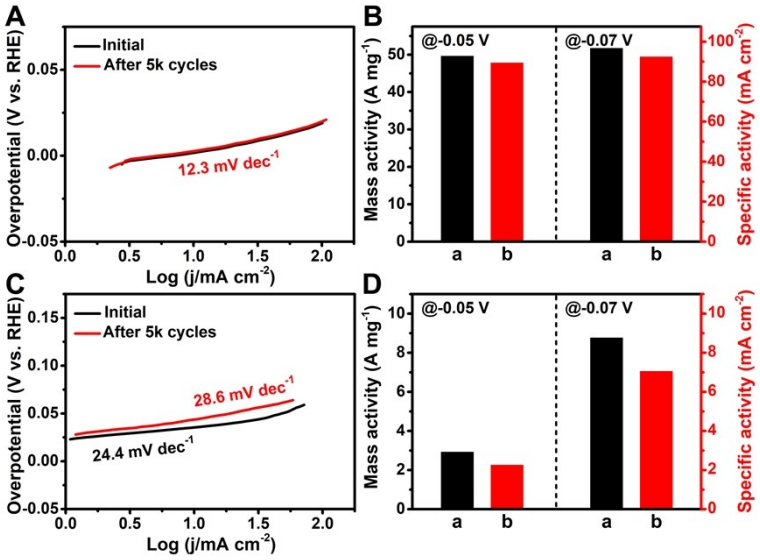

As shown in **Figure S40A**, the as-prepared $S_{6.5}$-doped $Au_{77.6}/Pd_{0.8}/Pt_{15.1}$ aerogel show a negligible change in their Tafel plot before and after the ADT tests of 5k cycles and so do their Tafel slopes. In contrast, commercial Pt/C catalysts display an obvious change in their Tafel plots and their Tafel slopes were increased from 24.4 to 28.6 mV dec^{-1} **(Figure S40C)**. Moreover, the mass activity (at -0.05 V) of the as-prepared $S_{6.5}$-doped $Au_{77.6}/Pd_{0.8}/Pt_{15.1}$ aerogel was 96.5% of the initial one before and after the ADT tests of 5k cycles, while that of commercial Pt/C catalysts was 77.1% of the initial one **(Figure S40B and D)**. Furthermore, the current density (at -0.07 V) of the as-prepared $S_{6.5}$-doped $Au_{77.6}/Pd_{0.8}/Pt_{15.1}$ aerogel was 95.6% of the initial one after the ADT tests of 5k cycles while that of commercial Pt/C catalysts was 80.2% of the initial one **(Figure S40B and D)**.

Therefore, the long-term stability of the as-prepared $S_{6.5}$-doped $Au_{77.6}/Pd_{0.8}/Pt_{15.1}$ aerogel towards the HER in acidic media is much better than that of commercial Pt/C catalysts.

Figure S41. Comparison in the electrocatalytic performance of the prepared $S_{6.5}$-doped $Au_{77.6}/Pd_{0.8}/Pt_{15.1}$ aerogel towards the alkaline HER with that of other Pt-based electrocatalysts reported in the literature.

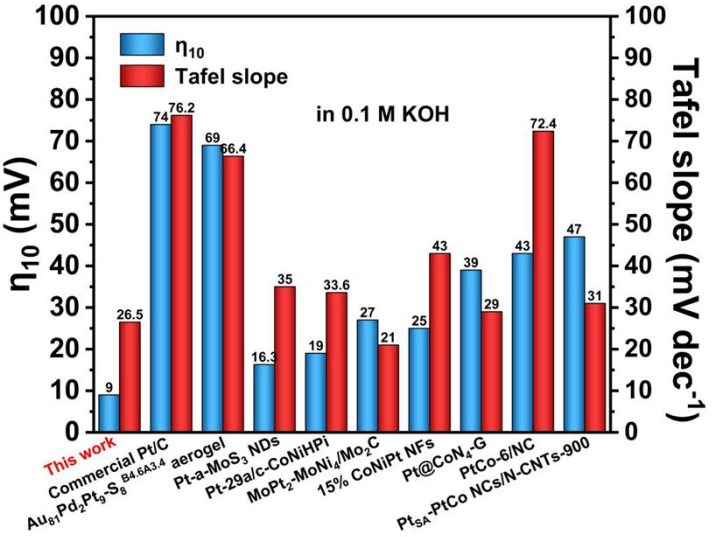

Figure S42. Comparison in the electrocatalytic performance of the prepared $S_{6.5}$-doped $Au_{77.6}/Pd_{0.8}/Pt_{15.1}$ aerogel towards the acidic HER with that of other Pt-based electrocatalysts reported in the literature.

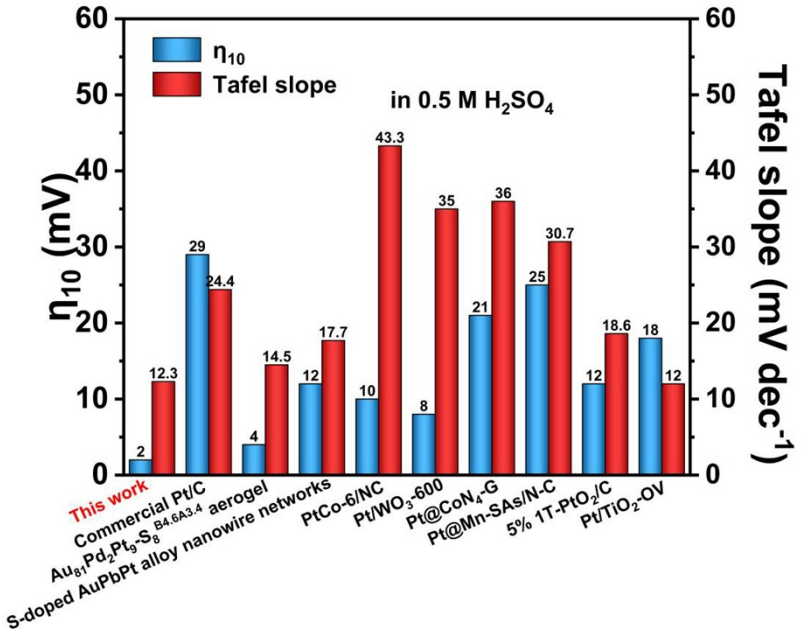

Table S1. Summarized data of the elemental composition of the as-prepared $S_{6.5}$-doped $Au_{77.6}/Pd_{0.8}/Pt_{15.1}$ aerogel on the basis of ICP-AES results.

Samples	Au %	Pd %	Pt %	S %
$S_{6.5}$-doped $Au_{77.6}/Pd_{0.8}/Pt_{15.1}$ aerogel	77.4	0.9	15.1	6.6

The percentages of each element are derived from the corresponding mass concentration of Au, Pd, Pt, and S element in the as-prepared $S_{6.5}$-doped $Au_{77.6}/Pd_{0.8}/Pt_{15.1}$ aerogel (Au: 26.78 mg/L; Pd: 0.17 mg/L; Pt: 5.17 mg/L; S: 0.37 mg/L).

Table S2. Summarized data of CO stripping tests measured in the acidic media of commercial Pd/C catalysts, a series of S-doped AuPdPt aerogel, and commercial Pt/C catalysts. These S-doped AuPdPt aerogels were prepared under different molar ratios of Pd(II)-to-Pt(IV): 1:10, 1:13, 1:17, 1:20.

Samples	E_{onset} [V]	Lower peak position [V]	Higher peak position [V]	$ECSA_{CO}$ [m^2 g^{-1}]
Commercial Pd/C catalysts	0.901	0.951	-	59.45
S-doped AuPdPt aerogel (Pd:Pt = 1:10)	0.656	0.779	1.015	113.21
S-doped AuPdPt aerogel (Pd:Pt = 1:13)	0.646	0.785	1.067	143.25
S-doped AuPdPt aerogel (Pd:Pt = 1:17)	0.643	0.780	1.061	165.41
S-doped AuPdPt aerogel (Pd:Pt = 1:20)	0.615	0.781	1.057	178.55
Commercial Pt/C catalysts	0.790	0.869	-	63.96

Table S3. Summarized XPS data of the Binding Energies (BEs) of the Au 4f, Pd 3d and Pt 4f orbitals of $S_{5.9}$-doped $Au_{79.2}/Pd_{0.8}/Pt_{14.1}$ aerogel, $S_{6.1}$-doped $Au_{78.2}/Pd_{0.8}/Pt_{14.9}$ aerogel, the as-prepared $S_{6.5}$-doped $Au_{77.6}/Pd_{0.8}/Pt_{15.1}$ aerogel and $S_{7.2}$-doped $Au_{76.2}/Pd_{0.8}/Pt_{15.8}$ aerogel. The BEs of the Au 4f, Pd 3d and Pt 4f orbitals of pure Au NPs, pure Pd NPs and pure Pt NPs are also shown for comparison.

Samples	Au(0)			Pd(0)			Pt(0)		
	Au $4f_{7/2}$ [eV]	Au $4f_{5/2}$ [eV]	ΔAu $4f_{7/2}$ [eV]	Pd $3d_{5/2}$ [eV]	Pd $3d_{3/2}$ [eV]	ΔPd $3d_{5/2}$ [eV]	Pt $4f_{7/2}$ [eV]	Pt $4f_{5/2}$ [eV]	ΔPt $4f_{7/2}$ [eV]
Pure Au NPs	84.2	87.9	0	-	-	-	-	-	-
Pure Pd NPs	-	-	-	335.0	340.3	0	-	-	-
Pure Pt NPs	-	-	-	-	-	-	71.0	74.3	0
$S_{5.9}$-doped $Au_{79.2}/Pd_{0.8}/Pt_{14.1}$ aerogel	83.84	87.54	-0.36	335.37	340.67	+0.37	71.93	75.23	+0.93
$S_{6.1}$-doped $Au_{78.2}/Pd_{0.8}/Pt_{14.9}$ aerogel	83.83	87.53	-0.37	335.36	340.66	+0.36	72.05	75.35	+1.05
$S_{6.5}$-doped $Au_{77.6}/Pd_{0.8}/Pt_{15.1}$ aerogel	83.82	87.52	-0.38	335.35	340.65	+0.35	72.13	75.43	+1.13
$S_{7.2}$-doped $Au_{76.2}/Pd_{0.8}/Pt_{15.8}$ aerogel	83.86	87.56	-0.34	335.37	340.67	+0.37	72.18	75.48	+1.18

Table S4. Comparison in the electrocatalytic performance of the as-prepared $S_{6.5}$-doped $Au_{77.6}/Pd_{0.8}/Pt_{15.1}$ aerogel and commercial Pt/C catalysts towards the HER in 0.1 M KOH solution.

Samples	η_{10} [mV]	$\Delta\eta_{10}$ [mV]	Tafel slope [mV dec^{-1}]	MA [A mg^{-1}]	SA [mA cm^{-2}]	j_0 [mA cm^{-2}]
$S_{6.5}$-doped $Au_{77.6}/Pd_{0.8}/Pt_{15.1}$ aerogel	9	65	26.5	9.74	9.51	4.89
Commercial Pt/C catalysts	74	0	76.2	0.25	0.67	0.86

Table S5. Comparison in the electrocatalytic performance of the as-prepared $S_{6.5}$-doped $Au_{77.6}/Pd_{0.8}/Pt_{15.1}$ aerogel and other Pt-based electrocatalysts towards the HER in 0.1 M KOH solution.

Samples	η_{10} [mV]	$\Delta\eta_{10}$ [mV]	Tafel slope [mV dec^{-1}]	References
$S_{6.5}$-doped $Au_{77.6}/Pd_{0.8}/Pt_{15.1}$ aerogel	9	65	26.5	This work
$Au_{81}Pd_2Pt_9$-$S_8^{B4.6A3.4}$ aerogel	69	5	66.4	[1]
Pt-a-MoS_3 NDs	16.3	13.7	35	[5]
Pt-a/c-CoNiHPi	19	31	33.6	[6]
$MoPt_2$-$MoNi_4/Mo_2C$	27	-	21	[7]
15% CoNiPt NFs	25	22	43	[8]
Pt@CoN_4-G	39	3	29	[9]
PtCo-6/NC	43	-	72.4	[10]
Pt_{SA}-PtCo NCs/N-CNTs-900	47	-	31	[11]
$Pt/Ti_3C_2O_x$	75	12	-	[12]

Table S6. Comparison in the electrocatalytic performance of the as-prepared $S_{6.5}$-doped $Au_{77.6}/Pd_{0.8}/Pt_{15.1}$ aerogel and commercial Pt/C catalysts towards the HER in 0.5 M H_2SO_4 solution.

Samples	η_{10} [mV]	$\Delta\eta_{10}$ [mV]	Tafel slope [mV dec^{-1}]	MA [A mg^{-1}]	SA [mA cm^{-2}]	j_0 [mA cm^{-2}]
$S_{6.5}$-doped $Au_{77.6}/Pd_{0.8}/Pt_{15.1}$ aerogel	2	27	12.3	49.6	96.7	6.33
Commercial Pt/C catalysts	29	0	24.4	2.92	8.76	0.48

Table S7. Comparison in the electrocatalytic performance of the as-prepared $S_{6.5}$-doped $Au_{77.6}/Pd_{0.8}/Pt_{15.1}$ aerogel and other Pt-based electrocatalysts towards the HER in 0.5 M H_2SO_4 solution.

Samples	η_{10} [mV]	$\Delta\eta_{10}$ [mV]	Tafel slope [mV dec^{-1}]	References
$S_{6.5}$-doped $Au_{77.6}/Pd_{0.8}/Pt_{15.1}$ aerogel	2	27	12.3	This work
$Au_{81}Pd_2Pt_9$-$S_8^{B4.6A3.4}$ aerogel	4	25	14.5	[1]
S-doped AuPbPt alloy nanowire networks	12	17	17.7	[13]
PtCo-6/NC	10	35	43.3	[10]
Pt/WO_3-600	8	17	35	[14]
Pt/MPNC	12	5.1	-	[15]
Pt@CoN_4-G	21	8	36	[9]
Pt@Mn-SAs/N-C	25	5	30.7	[16]
5% 1T-PtO_2/C	12	16	18.6	[17]
Pt/TiO_2-OV	18	17	12	[18]

References

[1] Y. Fan, X. Zhang, M. Zhang, X. Yue, W. Du and H. Xia, *Chem. Eng. J.* 2023, **470**, 144149.

[2] M. Yang, K. Zhou, C. Wang, M. Zhang, C. Wang, X. Ke, G. Chen, H. Wang and R. Wang, *J. Mater. Chem. A* 2022, **10**, 25692–25700.

[3] W. Huo, X. Zhou, Y. Jin, C. Xie, S. Yang, J. Qian, D. Cai, Y. Ge, Y. Qu, H. Nie and Z. Yang, *Small* 2023, 2207847.

[4] X. Zhang, J. Wang, M. Zhang, X. Yue, W. Du, W. Fan and H. Xia, *J. Mater. Chem. A* 2022, **10**, 7800–7810.

[5] K. Guo, J. Zheng, J. Bao, Y. Li and D. Xu, *Small* 2023, **19**, 2208077.

[6] Y. Li, X. Zhang, L. Liu, H. Sheng, C. Li, L. Cao, H. Li, C. Xia and B. Dong, *Small* 2023, **19**, 2300368.

[7] H. Zhang, P. Song, P. Yao, D. Zhang, J. Cao, X. Gong, C. Han and W. Xu, *Chem. Eng. J*. 2023, **470**, 144375.

[8] Y. Pan, J. Gao, E. Lv, T. Li, H. Xu, L. Sun, A. Nairan and Q. Zhang, *Adv. Funct. Mater.* 2023, **33**, 2303833.

[9] M. Zhang, H. Li, J. Chen, F.-X. Ma, L. Zhen, Z. Wen and C.-Y. Xu, *Adv. Funct. Mater.* 2023, **33**, 2303189

[10] M. Zhang, T. Zhou, D. Bukhvalov, F. Han, C. Wang and X. Yang, *Appl. Catal. B Environ.* 2023, **337**, 122976.

[11] W. Chen, X. Zhu, W. Wei, H. Chen, T. Dong, R. Wang, M. Liu, K. (Ken) Ostrikov, P. Peng and S.-Q. Zang, *Small* 2023, **19**, 2304294.

[12] H. Hong, H. Y. Kim, W. I. Cho, H. C. Song, H. C. Ham, K. Chae, F. M. Mota, J. Y. Kim and D. H. Kim, *J. Mater. Chem. A* 2023, **11**, 5328–5336.

[13] X. Zhang, S. Wang, C. Wu, H. Li, Y. Cao, S. Li and H. Xia, *J. Mater. Chem. A* 2020, **8**, 23906–23918.

[14] X. Fan, C. Liu, B. Gao, H. Li, Y. Zhang, H. Zhang, Q. Gao, X. Cao and Y. Tang, *Small* 2023, **19**, 2301178.

[15] Z. Zeng, S. Küspert, S. E. Balaghi, H. E. M. Hussein, N. Ortlieb, M. Knäbbeler-Buß, P. Hügenell, S. Pollitt, N. Hug, J. Melke and A. Fischer, *Small* 2023, **19**, 2205885.

[16] L. Gong, J. Zhu, F. Xia, Y. Zhang, W. Shi, L. Chen, J. Yu, J. Wu and S. Mu, *ACS Catal.* 2023, **13**, 4012–4020.

[17] H. Yang, Y. Ji, Q. Shao, W. Zhu, M. Fang, M. Ma, F. Liao, H. Huang, Y. Zhang, J. Yang, Z. Fan, Y. Li, Y. Liu, M. Shao and Z. Kang, *Energy Environ. Sci.* 2023, **16**, 574–583.

[18] Z. Wu, P. Yang, Q. Li, W. Xiao, Z. Li, G. Xu, F. Liu, B. Jia, T. Ma, S. Feng and L. Wang, *Angew. Chem. Int. Ed.* 2023, **62**, e202300406.